

Amsterdam University College

Capstone / Bachelor Thesis

Dutch Solar Cell Performance:

*The efficiency and Shockley-Queisser limits of various solar panels
under Dutch weather conditions*

*Ruby de Hart (AUC)
Science Major*

25-05-2016

*Supervisor: Forrest Bradbury (AUC)
Co-supervisor: Bruno Ehrler (FOM Institute AMOLF)*



Abstract

This thesis evaluates the performance of six different types of solar panels under Dutch weather conditions through observed efficiency and theoretical maximum efficiency. In contrast to the rainy dreary Netherlands, the present literature body mainly conducts research on solar panel efficiencies in hot and sunny climates. It generally fails to discuss the influence of low irradiance and humid conditions on the observed efficiency as well as the impact of environmental conditions on the theoretical maximum efficiency. In order to investigate these environmental influences and their impact on both the observed and theoretical efficiency, this study focuses on the performance of different panels located in the Netherlands while providing calculated values of the theoretical maximum efficiency simultaneously. The research site consists of six distinct solar cell structures, which include three distinct semiconductor materials, and measurement equipment for the weather, spectrum, irradiance, and current-voltage curve parameters. The materials are copper indium gallium selenide, cadmium telluride, and silicon. This thesis thus compares the observed and theoretical efficiencies of the six solar panels and evaluates their relation to various environmental conditions, such as module temperature, irradiance, and average photon energy. The high relative humidity in the Netherlands did not show a significant influence on performance while the difference between sunny and cloudy days was distinct: high theoretical efficiencies were calculated for the cadmium tellurium solar panel while the other panels had clearly lower efficiencies under cloudy circumstances. However, this trend was not visible in the observed efficiency even though the pyranometer and the integrated spectra arrived at much the same irradiance values. Furthermore, sunny and cloudy days had different dependences of measured efficiency on the average photon energy.

Content

1. <u>Introduction</u>	p. 4
2. <u>Background Physics</u>	p. 5
2.1. <u>Semiconductor physics</u>	p. 5
2.2. <u>Influences of spectrum in the solar cell</u>	p. 8
2.3. <u>Temperature effect on performance</u>	p. 8
2.4. <u>Photovoltaics parameters and IV curves</u>	p. 8
2.5. <u>Shockley-Queisser Limit</u>	p. 10
2.6. <u>Standard Test Conditions</u>	p. 12
3. <u>Background Atmospheric and Climate Science</u>	p. 13
3.1. <u>Atmospheric effects on irradiance and spectrum</u>	p. 13
3.2. <u>The Dutch Climate</u>	p. 13
4. <u>Methodology</u>	p. 15
4.1. <u>Solar field at AMOLF setup and specifics</u>	p. 15
4.2. <u>Data Analysis</u>	p. 17
5. <u>Results</u>	p. 19
5.1. <u>Pyranometer and Spectrometer Irradiance</u>	p. 19
5.2. <u>Temperature Dependence</u>	p. 20
5.3. <u>Irradiance Dependence</u>	p. 21
5.4. <u>Spectral Changes</u>	p. 22
5.5. <u>Weather Variations</u>	p. 26
5.6. <u>Best Performing Solar Panel</u>	p. 27
5.7. <u>Influence of Average Photon Energy</u>	p. 30
5.8. <u>Influence of Relative Humidity</u>	p. 31

6. Discussion and Conclusion	p. 32
6.1. Environmental Conditions	p. 32
6.2. Observed Efficiency versus Shockley-Queisser Limit	p. 32
6.3. Dutch Humidity	p. 32
6.4. Outliers	p. 33
6.5. Comparing Solar Panels	p. 33
6.6. Limitations	p. 33
6.7. Conclusion and Future Research	p. 34
6.8. Acknowledgements	p. 35
Bibliography	p. 36
Appendix 1: Data Collection Circuit and Software System Overview	p. 38
Appendix 2: Mathematica Code	p. 39
Appendix 3: Data List Layout	p. 42

1. Introduction

Every hour the Earth receives the amount of energy from the Sun that humanity consumes in one year (Perez and Perez 2009), which makes solar energy a feasible renewable technology for energy generation for human use. However, less than 1% of energy consumed is generated by solar energy conversion (Sargent 2012). In order to increase this contribution to the energy market, solar energy needs to become more competitive. One of the ways in which to achieve this goal is by increasing the efficiency of the solar cells that convert solar energy into electrical energy. However, these solar cells are restricted by the so-called Shockley-Queisser limit. This causes the maximum efficiency of an ordinary single-junction solar cell to be about 33% at a bandgap of 1.34 eV. The Shockley-Queisser limit further assumes the ideal test conditions in laboratories, Standard Test Conditions (STC). However, a situation with these exact conditions occurs rarely and it is, therefore, important to test solar modules outside. Research with solar fields can explore the relation between STC performance and real performance by including the environmental conditions that influence the solar module efficiency. Examples of these various components are the total solar irradiance, the ratio of direct and diffuse radiation, the distribution of light's power in the electromagnetic spectrum, and the temperature. During winter the sun is low and the light thus has to travel through more air mass to get to the solar cell. A higher air mass causes more diffuse (and thus redder) light to reach the cell (PVeducation 2013). Different cells respond differently to the varying colours of light and, therefore, some might be better suited for locations and times with a lower sun position in the sky. Additionally, previous research has shown that weather influences the performance of solar panels in the way of clouds, wind speed, relative humidity (mostly with respect to degradation), and temperature (e.g. Emziane and Altal 2012; Touati et al. 2012). Especially the impact of temperature has been researched extensively. However, this has mostly been done in countries with hot and relatively clear-sky climates.

In contrast to the main body of literature, this work is conducted in the Netherlands at FOM Institute AMOLF, which is located in Amsterdam-Oost. The Dutch climate has both diffuse solar radiation and relatively low temperatures and is thus different compared to the majority of solar field research so far. This thesis thus aims to evaluate the influence of the Dutch weather conditions on the efficiency and power output of different solar modules. Additionally, it compares the measured solar module efficiency to the theoretical efficiency limit at the module's band gap and the detected spectrum using the theory of Shockley and Queisser. To evaluate this an understanding of semiconductor physics for solar cells as well as of atmospheric and climate influences on irradiance, spectra, and weather is necessary. Therefore, this thesis consists of the following components: background physics (2), background atmospheric and climate science (3), methodology (4), results (5), and discussion and conclusion (6).

2. Background Physics

2.1. Semiconductor physics

Crystalline materials are collections of atoms where the electrons have split into two approximately continuous electron bands: the valence band and the conduction band (Ashcroft and Mermin 1976; Neamen 2012). The energy difference between these two bands is called the energy gap or “bandgap”. At 0 K temperature the valence band houses all electrons, while the conduction band is empty and has a higher energy. The valence band is either completely filled (when the fermi level is outside the band) or partly filled with electrons (when the fermi level lies inside the valence band) depending on the type of band splitting (Figure 1) (Neamen 2012).

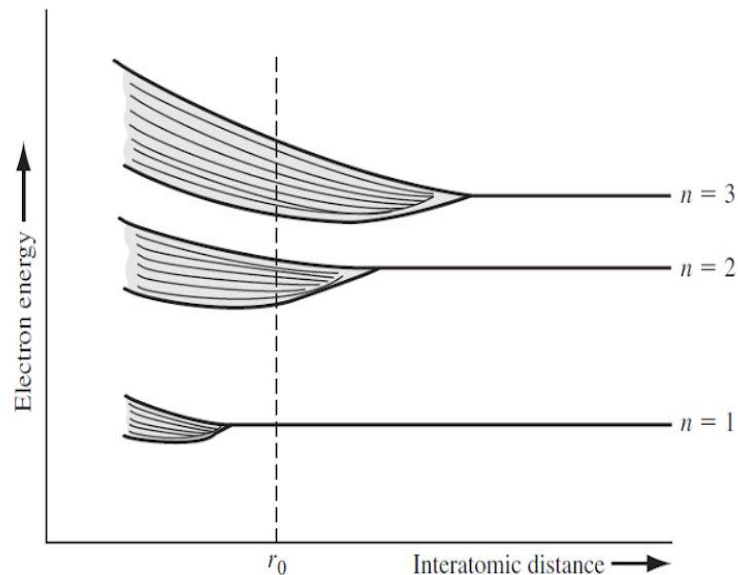


Figure 1: Energy band splitting (Neamen 2012).

Band splitting can occur in various ways resulting in different material categories: metals, semiconductors, and insulators (Figure 2; Averill and Eldredge 2012). Metals have their fermi level inside of the valence band, making it easy to thermally excite electrons into higher energy states. This makes the electrons more mobile and causes metals to be good conductors. Both semiconductors and insulators have their fermi levels above the valence band. For these materials electrons can only be excited into higher energy states when they receive an energy equivalent to the bandgap. The bandgap is very large for insulators - usually between 3.5 and 6 eV or larger - making it hard for electrons to be excited (Neamen 2012). In semiconductors the bandgap is smaller (generally less than 2 eV) and it is possible to excite electrons thermally or radiatively (Ashcroft and Mermin 1976). In the former heat causes the electrons to obtain the energy for excitation, while in the latter a photon causes the electron to get the right amount of

energy to reach the conduction band. Photovoltaics uses this principle of photo-excitation to generate electricity from incident sunlight.

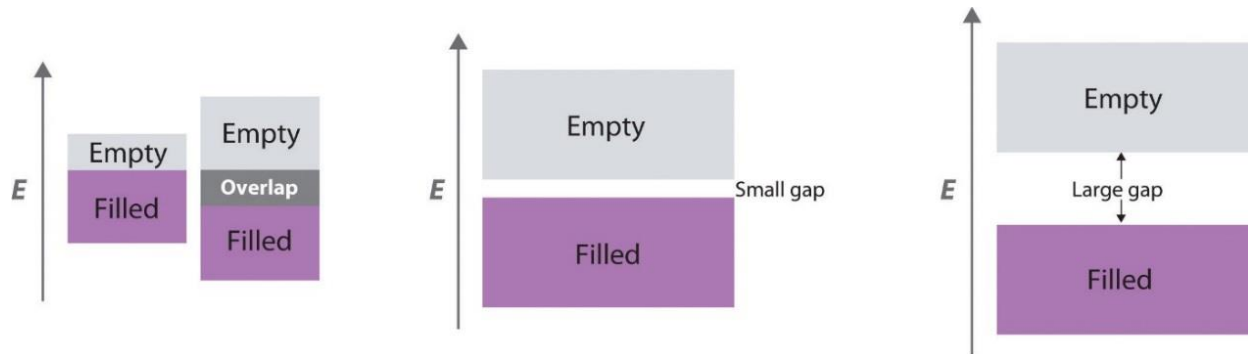


Figure 2: Simplified band structures of metals (left), semiconductors (middle), and insulators (right) (Averill and Eldredge 2012).

Before elaborating on the different device parameters of a solar cell, it is necessary to explain photo-excitation in more detail. Light can be described as particles, photons, and as waves. The energy E of light depends on its wavelength λ where a high wavelength corresponds to a low energy:

$$E = \frac{hc}{\lambda} = hf. \quad (1)$$

Where h is Planck's constant, c is the speed of light and f the frequency of the light wave. When interacting with electrons, light is best considered as a particle with a distinct energy. The excitation of electrons from the valence band into the conduction band can only take place when the incoming light has enough energy to bridge the bandgap. If this is not the case and the light has too little energy - or is "too red" - the electron will not be excited and the photon is not absorbed. If the incoming photon has enough energy, the electron is excited and leaves behind a hole, which in its own turn is also a charge carrier but of positive charge. However, if the photon energy and the bandgap energy are not a perfect match and the photon has some excess energy this is lost in the form of heat. Therefore, both too-low-energy photons and too-high-energy photons cause the efficiency of the solar cell to decrease with respect to the ideal efficiency. Figure 3 depicts an electron photo-excitation, wherein an electron is excited out of the valence band into the conduction band, in two dimensions.

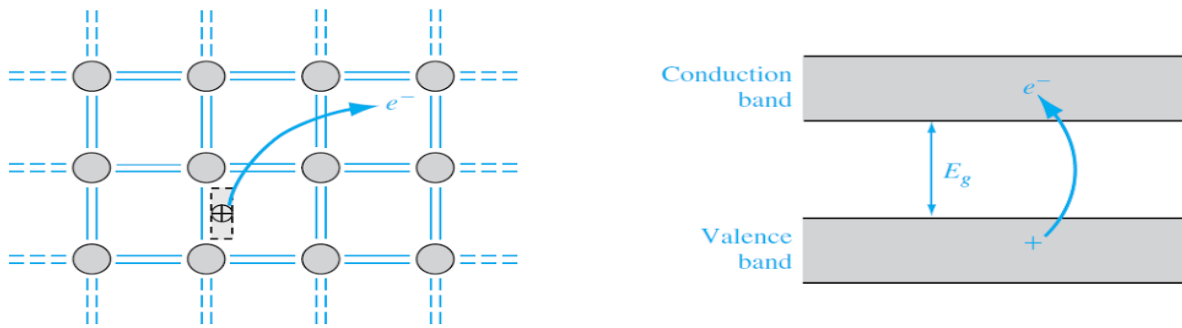


Figure 3: Excitation of an electron out of a covalent (valence) band into the conduction band (Neamen 2012).

The solar cell operation is often enhanced by so-called “doping” of the material. Hereby atoms with either more or less electrons are implemented into the semiconductor material. In the case of silicon, which is the most widely used material for solar cells, these are often phosphorus and boron, respectively. Donor atoms – impurities – have one electron more than the host material; the binding energy of this electron is small compared to the bandgap and thus create an additional energy level just below the conduction band (Ashcroft and Mermin 1976). Acceptor atoms, which have an “extra” hole or one electron less, cause the addition of an energy level just above the valence band in a similar manner. Therefore, doping alters the band structure of the semiconductor by either having more free electrons or more free holes before excitation (Figure 4). This, in turn, also influences the chemical potential.

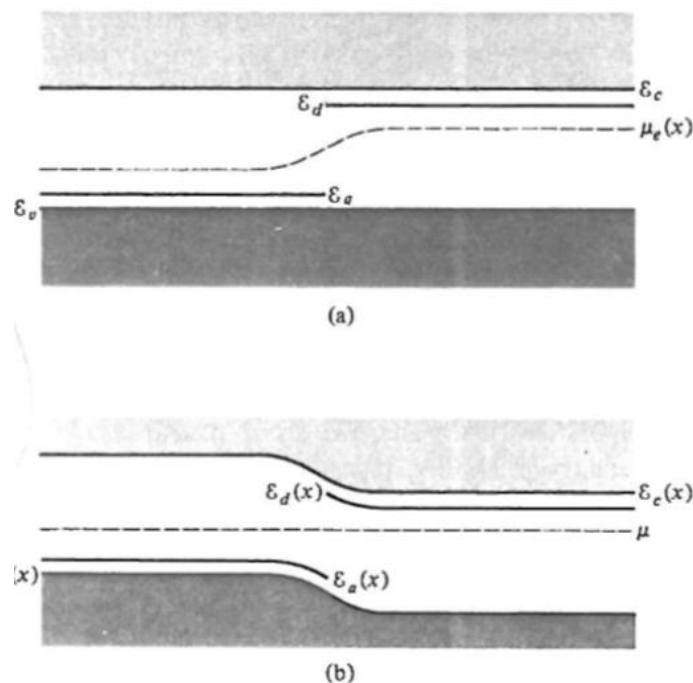


Figure 4: Band structure of a semiconductor including donor and acceptor energy levels and the chemical potential. Constant energy levels (a) correspond to a varying chemical potential and vice versa (b) (Ashcroft and Mermin 1976).

2.2. Influences of spectrum on the solar cell

The energy needed for photon excitation in solar cells comes from an entire spectrum of photon energies varying from ultraviolet to infrared. As aforementioned, only photons with an energy that is equal or greater than the bandgap energy of the semiconductor can be absorbed. Therefore, for the same semiconductor, a red spectrum, which has a lower average photon energy (APE), will be less efficient than a blue spectrum with higher APE (PV Education 2013). This also means that for semiconductors with different bandgaps the spectral response varies. A semiconductor with a large bandgap will need photons of higher energy in order for excitation to take place, while a small bandgap semiconductor can absorb at longer wavelengths. Solar cells with a small bandgap might thus be more effective at a spectrum with low APE and vice versa.

2.3. Temperature effect on performance

At absolute zero, $-273.15\text{ }^{\circ}\text{C}$, no electrons in the valence band of a semiconductor can gain the energy to be excited into the conduction band and the material is thus in equilibrium. However, with temperatures above this point, electrons can spontaneously be excited and leap to the conduction band as they can gain energy from the lattice vibrations of the material. When the temperature further increases, the amount of spontaneously excited electrons also grows (Neamen 2012). One would expect the efficiency for a semiconductor solar cell to thus increase with rising temperature. However, the higher thermal energy of the material causes more lattice vibrations. These will decrease the mobility of the electron, making it harder to be transported through the conduction band. In most cases the latter tendency is stronger and the solar cell efficiency thus decreases with increasing temperature (Kaldellis et al. 2014; Shaltout 2000; PV Education 2013). A warmer environment thus negatively impacts the efficiency of solar cells (Kaldellis et al. 2014)

2.4. Photovoltaics parameters and IV curves

Current-voltage (IV) curves give all important parameters of a solar cell to indicate its performance: the open-circuit voltage (V_{oc}), the short-circuit current (I_{sc}), the fill factor (FF), and the maximum power point (MPP) (PV Education 2013; Saetre et al. 2011). As a solar cell is a diode, the current-voltage (IV) curve is a combination of a (dark) diode curve and a photogenerated current (PV Education 2013). The diode law is thus adapted to become the following:

$$I = I_0 \left(e^{\frac{qV}{kT}} - 1 \right) - I_L. \quad (2)$$

Here I_0 and I_L represent the dark current and the light current, respectively, q is the electron charge, V is the voltage, k the Boltzmann constant, and T the temperature. IV measurements are determined by varying the load resistance on the solar cell and measuring the corresponding current through the cell (Piliouguine et al. 2011). The load resistance causes a different voltage over the cell and thus also changes the current. In this way, one can find the current and voltage that give the maximum power of the solar cell. The *MPP* gives the voltage at which the solar cell needs to operate to convert the largest amount of solar power into electrical energy (P_{max}). At *MPP* the so-called characteristic resistance, the output resistance of the solar cell, is equal to the resistance of the load. The characteristic resistance is calculated by dividing the voltage at *MPP* by the current at *MPP*. An example of a diode IV curve is shown in Figure 5 together with the power density (current \times voltage).

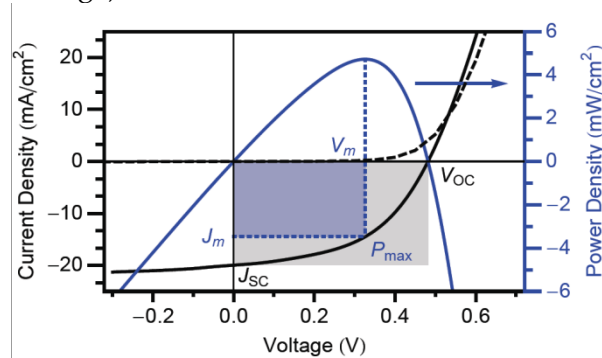


Figure 5: Example IV curve together with the power density (Ehrler 2012).

The V_{oc} is the voltage on the solar cell when there is no current flowing while the I_{sc} is the current when there is no voltage applied to the solar cell (Saetre et al. 2011). The V_{oc} and I_{sc} form the basis of the current-voltage (*IV*) curves. A perfect rectangular shape of these *IV* curves would mean maximum practical efficiency as the *MPP* would be at maximum possible current (I_{sc}) and maximum possible voltage (V_{oc}). However, this is thermodynamically impossible and thus is the maximum power point, the combination of current and voltage that gives the highest power, is located at a lower voltage and current than the V_{oc} and I_{sc} (PV Education 2013; Saetre et al. 2011). The ratio of power at *MPP* over I_{sc} times V_{oc} is known as the fill factor, a measure of the “squareness” of the *IV* curve (PV Education 2013). From an *IV* curve one cannot only find the power output of the solar cell, but also the role of different resistances. The two main resistances for a solar cell are the shunt and series resistances (PV Education 2013). These resistances mainly reduce *FF* and thus the efficiency of the solar cell (Figure 6).

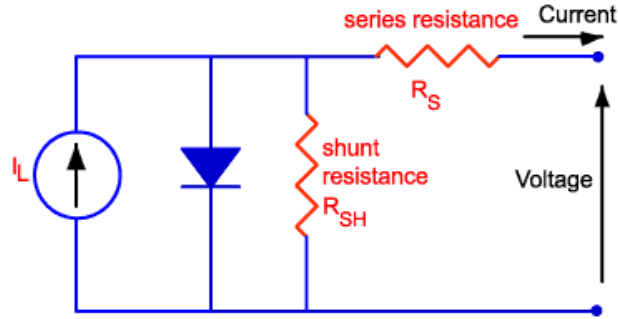


Figure 6: Schematic of a diode and its series and shunt resistances (PV Education 2013).

Series resistance (R_s) originates in three causes: movement of current, contact resistance, and resistance between the contacts and the semiconductor material (PV Education 2013). Incorporating series resistance in the function for current gives (Hanna and Nozik 2006; Neamen 2012):

$$I = I_L - I_0 e^{\frac{q(V+I R_S)}{kT}}. \quad (3)$$

This resistance reduces the slope of the IV curve near the V_{oc} and thus moves the MPP towards lower voltages. Whereas series resistance should be kept low, a low shunt resistance (R_{SH}) causes an alternative route for current to flow through; this reduces the current through the solar cell, therefore decreasing the voltage, and thus the solar cell efficiency. Adding shunt resistance to the diode law results in (Hanna and Nozik 2006; Neamen 2012):

$$I = I_L - I_0 e^{\frac{qV}{kT}} - \frac{V}{R_{SH}}. \quad (4)$$

At low light intensity there is less photogenerated current and the impact of a shunt resistance is greater. The same can be said for highly resistive solar cells at low voltage due to the fact that shunt resistances are parallel to the solar cell.

2.5. Shockley-Queisser Limit

The Shockley-Queisser (SQ) limit is the theoretical maximum efficiency that can be achieved by a solar cell with a certain bandgap and at Standard Testing Conditions (see next section). It was calculated by Shockley and Queisser in 1960 (Shockley and Queisser 1961) and states that the efficiency of a solar cell cannot exceed a certain value for multiple reasons: only photons with an energy above the bandgap can be absorbed (“incomplete absorption”), excess energy from high energy photons will be lost (“thermalisation”), blackbody radiation causes spontaneous emission of photons (“thermodynamic loss”), and a small fraction of carriers will recombine (through “radiative recombination”) (Hanna and Nozik 2006). Thermodynamic loss can also be understood from the band structure of the doped semiconductor. As explained in Section 2.1,

doping of the semiconductor decreases the effective bandgap, which causes a leakage current or “dark current” (Polman et al. 2016). This thus decreases the voltage that can be extracted. These limiting factors, also called the detailed balance model, are summarized in Figure 7.

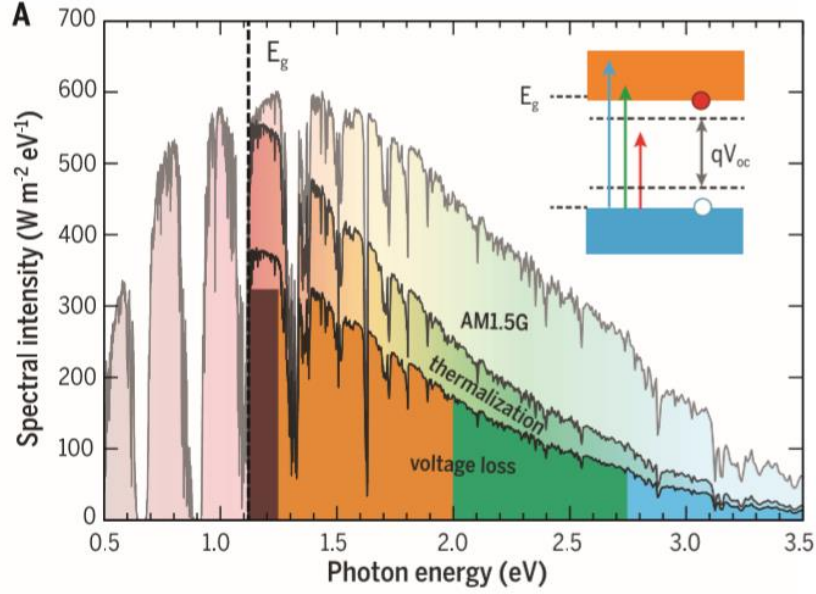


Figure 7: Stepwise construction of the limitations to the efficiency from the AM 1.5 spectrum (Polman et al. 2016).

Mathematically, the SQ limit can be expressed as follows:

$$\eta(V) = \frac{J(V)V}{P}, \quad (5)$$

where J is equal to the current, V represents the operating voltage of the semiconductor, and P is the irradiance. The current consists of a photogenerated current and a recombination current that can both be calculated by integrating over the spectrum with respect to photon energy in the following two ways, respectively:

$$J_G(Eg) = q \int_{Eg}^{E_{max}} \Gamma(E) dE \quad (6)$$

$$J_R(V, Eg) = qg \int_{Eg}^{\infty} \frac{E^2}{\exp\left\{\frac{[E-qV]}{kT}\right\} - 1} dE. \quad (7)$$

These two currents, the photogenerated current and the radiative emission current, then combine into the total current of the solar cell as follows:

$$J(V, Eg) = J_G(Eg) - J_R(V, Eg). \quad (8)$$

2.6. Standard Test Conditions

The Standard Test Conditions (STC) are the universal conditions under which solar cells are examined for their performances (NREL 2016). Therefore, STC provide a way in which to assess the solar cell efficiency in a consistent manner throughout research thus ensuring that reported efficiencies are recorded under the same circumstances. The conditions under STC are the following (NREL 2016, PV education 2013):

- 25 °C cell operating/cell temperature;
- Air mass (AM) 1.5 or the “global spectral irradiance distribution by the American Society for Testing Materials” (G173-03);
- One sun illumination (1000 W/m²).

3. Background Atmospheric and Climate Science

3.1. Atmospheric effects on irradiance and spectrum

Atmospheric effects have several impacts on the solar radiation at the Earth's surface. The major effects for photovoltaic applications are the following (PV education 2013):

- a reduction in the power of the solar radiation due to absorption, scattering and reflection in the atmosphere;
- a change in the spectral content of the solar radiation due to greater absorption or scattering of some wavelengths;
- the introduction of a diffuse or indirect component into the solar radiation;
- local variations in the atmosphere (such as water vapour, clouds and pollution) which have additional effects on the incident power, spectrum and directionality.

As solar radiation passes through the atmosphere, gasses, dust and aerosols absorb the incident photons (Hobbs 2000). Specific gases, notably ozone (O_3), carbon dioxide (CO_2), and water vapour (H_2O), have very high absorption of photons that have energies close to the bond energies of these atmospheric gases. This absorption yields deep troughs in the spectral radiation curve. While the absorption by specific gasses in the atmosphere changes the spectral content of the terrestrial solar radiation, they have a relatively minor impact on the overall power (PV education 2013). Instead, the major factor reducing the power from solar radiation is the absorption and scattering of light due to air molecules and dust (Hobbs 2000; PV education 2013). This absorption process does not produce the deep troughs in the spectral irradiance, but rather causes a power reduction dependent on the path length through the atmosphere. This path length is often expressed in terms of the relative air mass the light has to travel through to reach the Earth's surface, where AM 1 refers to the sun being directly overhead. With AM 1, the absorption due to these atmospheric elements causes a relatively uniform reduction across the visible spectrum, so the incident light appears white. However, for longer path lengths, higher energy (lower wavelength) light is more effectively absorbed and scattered. Hence in the morning and evening the sun appears much redder and has a lower intensity than in the middle of the day. As different cells respond differently to the varying colours of light, some might be better suited for locations and times with a lower sun position in the sky.

3.2. The Dutch Climate

These influences on total solar radiation and the spectrum of the light reaching the Earth's surface are not constant; they do not only vary with location, but also with time due to the influence of weather. Weather stations can measure a large range of meteorological conditions, such as temperature and humidity. The efficiency of solar cells tends to be negatively affected by temperature due to a small I_{sc} increase but a significant V_{oc} -decrease with temperature. Humidity might influence the incoming spectrum by causing more scattering in the

atmosphere, thus having a different effect on different solar cells. These two quantities are interesting for analysis in a country like the Netherlands, which has a Cfb climate. A Cfb climate in the Köppen-Geiger climate classification system (Kottek et al. 2006; Peel et al. 2007) corresponds with a “warm temperate” and “fully humid”, and has a warm summer. In more precise terms the Cfb climate refers to the temperature of the hottest months (April – September) being above 10 °C, the coldest months being between 0 and 18 °C, without a dry season, and with at least four months above 10 °C (Peel et al. 2007). This climate type is thus relatively cool and accompanied by a regular amount of rain. The consistent precipitation state of the Netherlands becomes clear when examining its amount of sunshine and rainy days. The country has limited amount of sunshine hours (~1600) and a large amount of rainy days (~130) every year (KNMI 2011; Compendium 2015). This is considerably cooler and wetter than the solar field testing locations in regions with a vastly different climate, such as in the Middle East, that have often been the subject of research (Emziane and Altal 2012; Touati et al. 2013; NREL 2016).

4. Methodology

4.1. Solar field at AMOLF setup and specifics

As mentioned in the introduction, this work is conducted at FOM Institute AMOLF in Amsterdam-Oost, the Netherlands. The solar field at AMOLF faces southward and stands just outside the research building, at an angle above ground of 30 degree. It consists of six different types of solar cell modules (their main features are shown in Figures 8 and 9, and Table 1 below). The six modules are the following:

- Module 1: Copper Indium Gallium Selenide (CIGS), a flexible module;
- Module 2: Cadmium Telluride (CdTe);
- Module 3: Polycrystalline Silicon (Poly-Si);
- Module 4: Integrated Back Contact Monocrystalline Silicon (IBC Si);
- Module 5: Heterojunction Intrinsic Layer Monocrystalline Silicon (HIT Si);
- Module 6: Copper Indium Gallium Selenide (CIGSm), a module where the solar cells have a reflective back contact or mirror (m) contact.

All these modules are currently cost-competitive and are therefore readily available on the market. In this paper the different modules will be referred to by their abbreviation from now on.

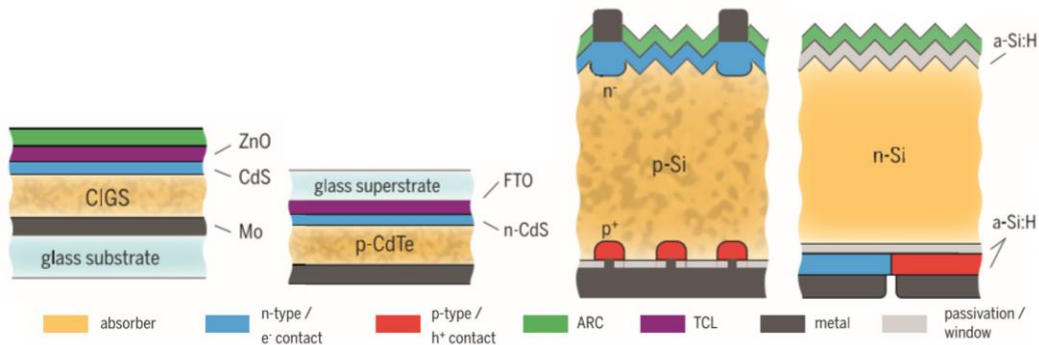


Figure 8: Four main solar cell architectures. From left to right: flexible CIGS (a reflective back layer results in module 6), CdTe, polycrystalline silicon, IBC silicon (with front contacts results in module 5) (Polman et al. 2016).

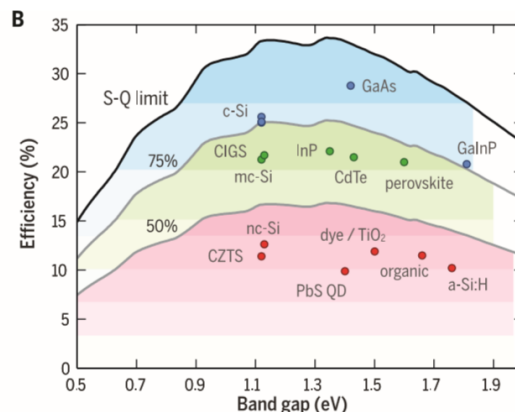


Figure 9: Record efficiency for high-, medium-, and low-efficiency semiconductor materials (Polman et al. 2016).

Module #	Name	Area (m ²)	Band Gap (eV)	Efficiency as stated by manufacturer (%)
1	Copper Indium Gallium Selenide (CIGS)	2.017 x 0.494	1.2 (NREL record)	12.7
2	Cadmium Telluride (CdTe)	1.200 x 0.600	1.45 (NREL record)	12.0
3	Polycrystalline Silicon (Poly-Si)	1.675 x 1.001	1.12	15.5
4	Integrated Back Contact Monocrystalline Silicon (IBC Si)	1.559 x 1.046	1.12	21.5
5	Heterojunction Intrinsic Layer Monocrystalline Silicon (HIT Si)	1.580 x 0.798	1.12	19.4
6	Copper Indium Gallium Selenide with back mirror (CIGSm)	1.656 x 0.656	1.2 (NREL record)	14.7

Table 1: the six solar cell modules at FOM Institute AMOLF including their areas, band gaps, and efficiencies.

The measurements analysed here started on 16-03-2016 and lasted until the end of April with data collection at every five minutes. The data collection includes three main groups: solar module parameters and current-voltage (*IV*) curves, weather data, and spectra. The first group of data is measured and collected by the solar field itself using PVscan 13 software from Ingenieurbüro Mencke & Tegtmeyer GmbH. This programme stores the *IV* curves and its main parameters (*I_{sc}*, *V_{oc}*, *P_{mpp}* and the corresponding current and voltage, *FF*, and *module temperature*). PVscan 13 calculates the *I_{sc}* and *V_{oc}* by extrapolation and the maximum power point (*MPP*) by multiplying the current with the voltage and uses a thermometer at the back of each panel to measure its temperature. A Compact Weather Station WS600-UMB from Lufft GmbH records multiple weather features: temperature, dew point, relative humidity, air pressure, air density, wind speed, and wind direction. All weather data are averaged over the five-minute measurement period. The influence of the weather features on the solar cell performance will be examined with emphasis on temperature and relative humidity as these weather components have the most direct impact on the incoming solar radiation (see Section 5.3). The spectra of the incoming solar radiation are measured by a MS-711 spectrometer by

EKO Instruments. This spectrometer measures between 300 and 1100 nm, which leaves out the tail-end of the infrared and part of the high energy photons. These now-excluded parts of the spectrum also contribute to the incoming irradiance. Through this exclusion the irradiance is thus currently underestimated, which results in higher relative power generated compared to the measured irradiance values. This measurement limitation therefore causes the theoretical efficiencies to be overestimated as the total power of this partial spectrum is much smaller than the complete irradiance. To resolve this issue, an interpolation based on the STC spectrum, AM 1.5, is done to include the spectrum from 1100 nm up to 4000 nm. The experimental results on the solar cell performance can then in turn be compared to the theoretical Shockley-Queisser limit for every individual module at any spectrum and temperature. This is accomplished by adjusting the Shockley-Queisser efficiency calculations for the different band gaps and the measured spectra. The module temperature is also included in this calculation as the operating temperature affects both the conductivity of charge carriers and the amount of excitations (see Section 2.3). A detailed explanation of the data analysis process is given in the following section. A full overview of the Data Collection Circuit and Software System can be found in Appendix 1.

4.2. Data Analysis

For data analysis all incoming data is processed in Mathematica. The parameter data is imported per module and per day after which the P_{mmp} (power at maximum power point) and irradiance are extracted from the data list. These are combined with the area of the relevant solar module to calculate the actual efficiency of the module:

$$\eta = \frac{P_{mmp}}{P \text{ (Irradiance)}}. \quad (9)$$

The SQ limits are calculated as stated in Sections 2.5 and 4.1. All modules have unique SQ limits at every point in time, even the ones with the same semiconductor material as their main component due to the different module temperatures. To examine the dependence between the composition of the incoming spectra and other parameters, the average photon energy (APE) of every spectrum is determined as follows:

$$APE = \frac{1}{q} \frac{\int E_{\lambda} d\lambda}{\int \Phi_{\lambda} d\lambda}, \quad (10)$$

where q is the electron charge, E is the energy per wavelength, and Φ_{λ} is the photon flux (Norton et al. 2015).

The Mathematica code thus includes the following main components (see Appendix 2 for part of the programme code and Appendix 3 for the Data List layout):

- Function Definitions;
- Spectra;
- Weather Data;

- Observed Efficiency;
- Ultimate Parameter List;
- Plots.

From these the temperature dependence, irradiance dependence, spectral changes, weather variations, best performing solar panel, the influence of average photon energy, and the influence of humidity is concluded (see Chapter 5).

5. Results

5.1. Pyranometer and Spectrometer Irradiance

As the observed efficiency is calculated using the irradiance values measured by the pyranometer and the Shockley-Queisser limit is based on data from the spectrometer – and thus also the irradiance as measured by it, Figure 10 shows the relation between the two irradiance values. The irradiance values show good correspondence with each other linearly and one to one; this ensures that the efficiency values are reliable. The outliers are likely caused by situations where the solar field was partially shaded, e.g. where the pyranometer was in the shade while the spectrometer was not shaded. These outliers will also show up as outliers in the other figures.

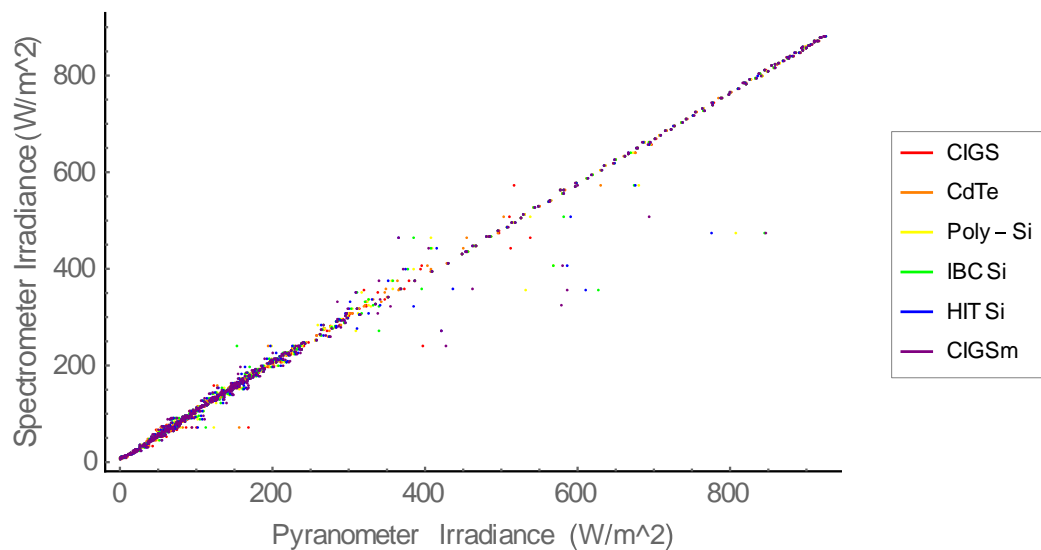


Figure 10: Pyranometer irradiance versus spectrometer irradiance

5.2. Temperature Dependence

As explained in Section 2.3, the temperature is expected to negatively affect the solar panel performance. To examine this, Figures 11 and 12 show the panel temperature versus the SQ limit and the measured efficiency. There is increased measurement noise in the mornings (at cold temperatures), which is due to the relatively high impact of small variations in measurement at low irradiance values. There is a bigger relative uncertainty, which causes noise.

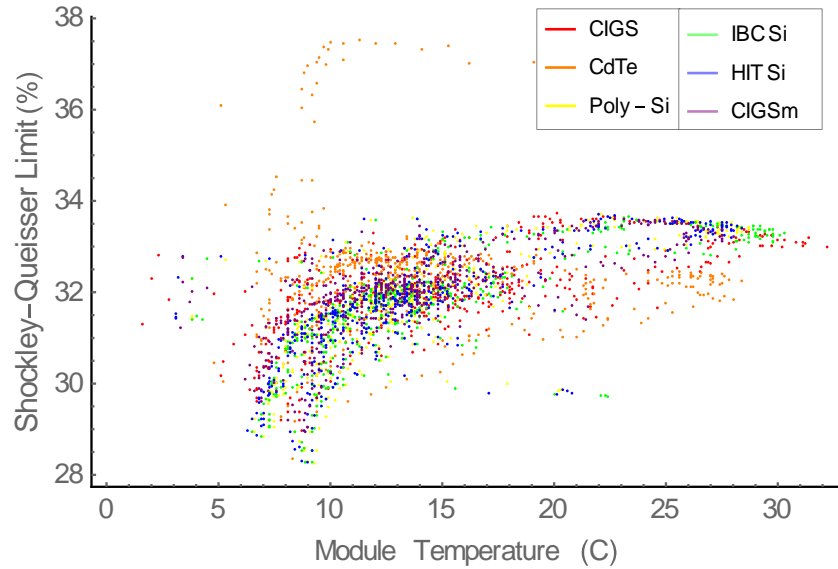


Figure 11: Module temperature versus Shockley-Queisser limit

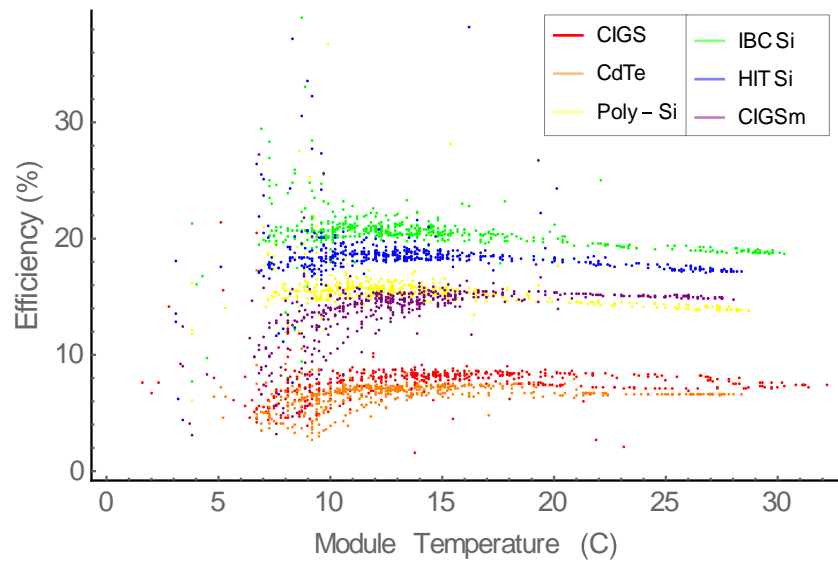


Figure 12: Module temperature versus observed efficiency

5.3. Irradiance Dependence

In Figures 13 and 14 it becomes clear that the irradiance dependence is as expected at low irradiance levels: the measured efficiency and SQ limit increase with increasing irradiance. At higher irradiance the SQ limit stays roughly constant (with a slight increase) while the measured efficiency increases. In the following sections (5.4, 5.6, and 5.7 specifically), this is shown in more detail that the spectrum shape changes with a larger amount of incoming solar radiation and the SQ limits and efficiencies are generally higher with large irradiance.

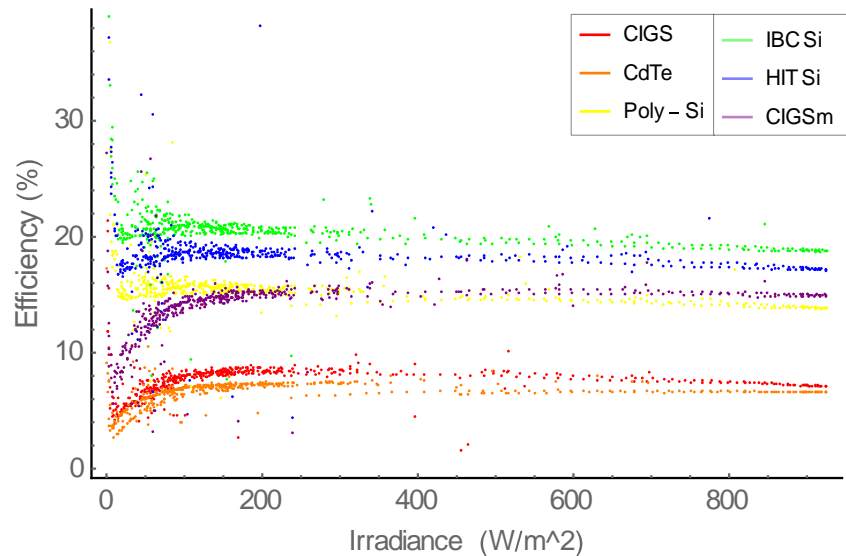


Figure 13: Irradiance versus observed efficiency

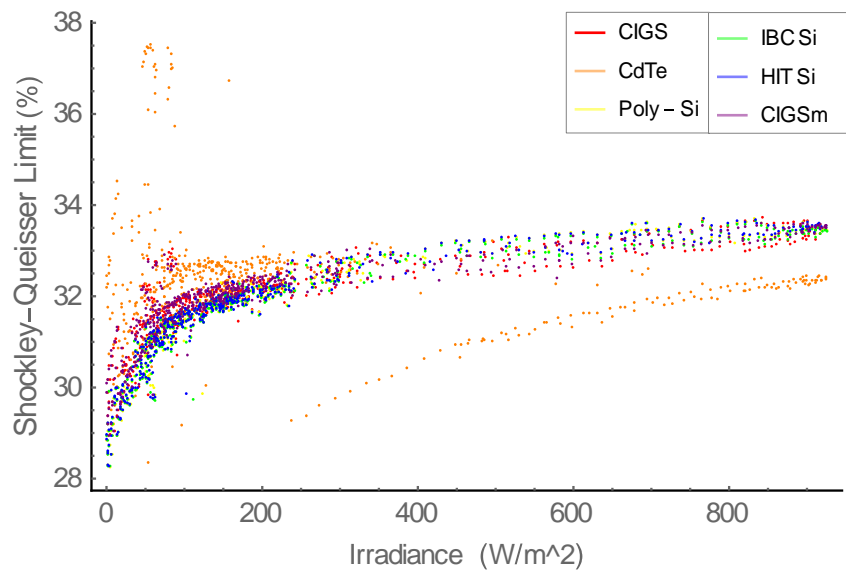


Figure 14: Irradiance versus Shockley-Queisser limit

5.4. Spectral Changes

Measurement of the spectra shows that there is large variation in two components: their shape and the area under the curve, the total irradiance. As expected, mornings and evenings have a lower irradiance which is explained by the solar position: less light reaches the solar panels due to the increase in air mass the light has to travel through. This already results in a large deviation from the STC. The shape of the spectra also varies during the day and between days. Early spectra, wherein the data is taken before 10:00, tend to be relatively flat; their peak is still located in the visible range, but at low irradiance values compared to the peaks of later spectra (Figures 15, 16, and 17). If a background signal would be present (ie noise in the dark), it would contribute significantly more to the spectrum at low irradiance levels than at large irradiance levels as its contribution would be relatively large. However, upon investigation, no significant background signal was found when measuring spectra in the dark.

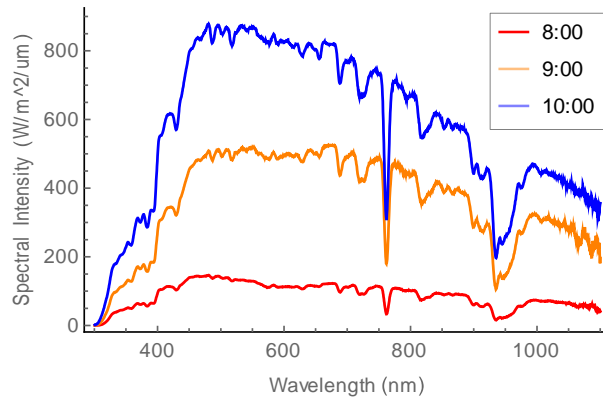


Figure 15: Various morning spectra on 17-03-2016

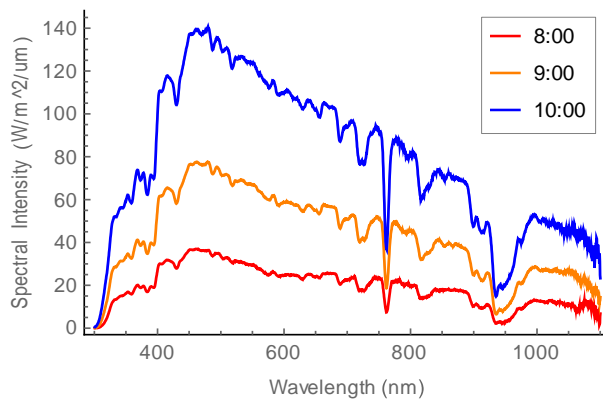


Figure 16: Various morning spectra on 18-03-2016

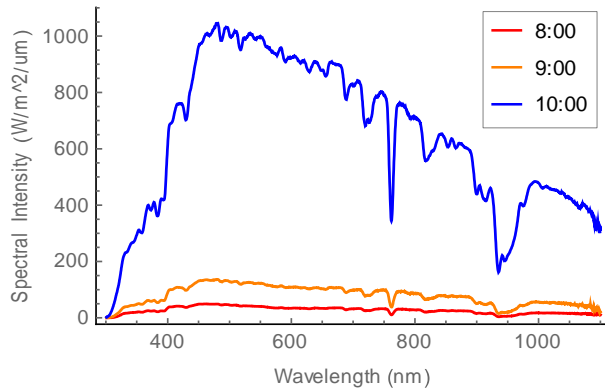


Figure 17: Various morning spectra on 23-03-2016

On the other hand, spectra with the largest irradiance values are quite similar in shape to the AM 1.5 spectrum and occur between 13:00 and 15:00 on sunny days (Figures 18 and 19).

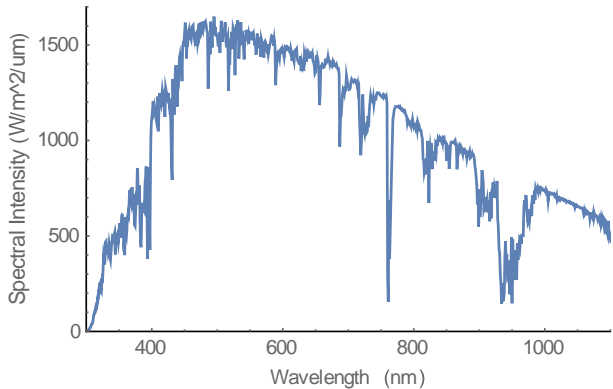


Figure 18: AM 1.5 spectrum

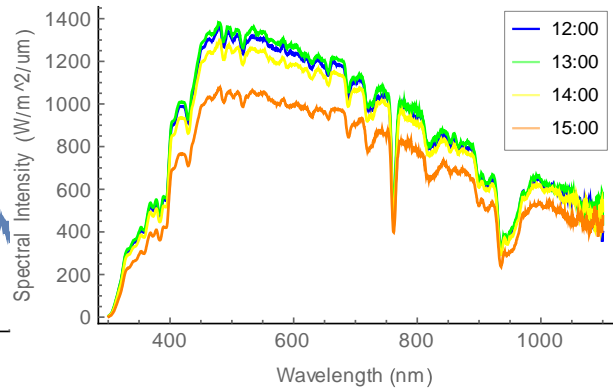


Figure 19: Various afternoon spectra on 17-03-2016

On cloudy or rainy days, when the irradiance is low, the spectra are slightly more peaked around 500 nm and show a more pronounced reduction in irradiance between 450 and 700 nm compared to the sunny case of the previous figure (Figures 20 and 21).

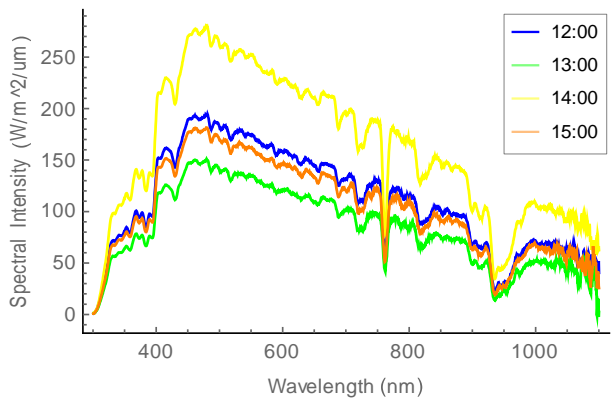


Figure 20: Various afternoon spectra on 23-03-2016

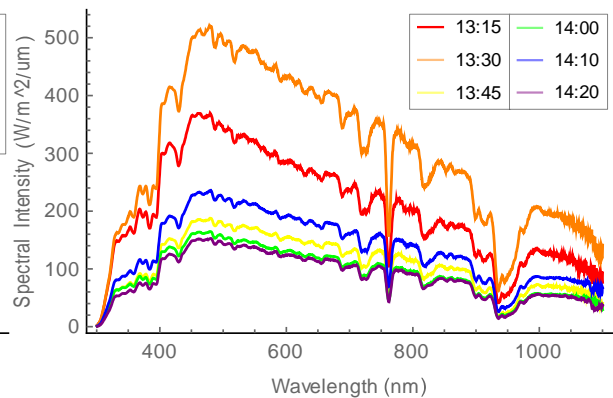


Figure 21: Various afternoon spectra on 18-03-2016

By calculating the average photon energy (APE) of every spectrum, it becomes clear how the time of the day – and thus the solar position – influences the incoming spectra on clear days (Figure 22). While 16-03-2016 and 17-03-2016 are significantly affected by the time of day, 21-03-2016 to 23-03-2016 were cloudy days and their spectra remain mostly constant over the entire day. Figure 22, 17-03-2016, also shows that an increase in APE is correlated with larger irradiances until about 1.42 eV; after this APE value the correlation becomes negative and the irradiance decreases towards larger APE values. Therefore, it becomes also clear that solar position is not the sole influencing factor on the APE (comparing Figures 22 and 23). If it were the only influence, there would be no high APE values at moments of low irradiance and thus there has to be a low irradiance, blue light impact that also plays a role.

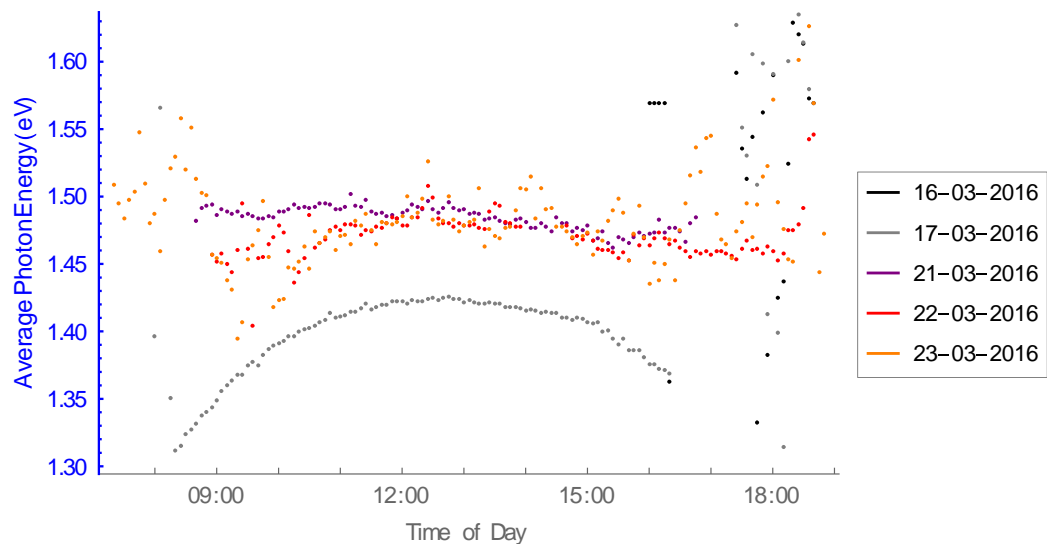


Figure 22: Average photon energy (up to 1.65 eV) over five measurement days

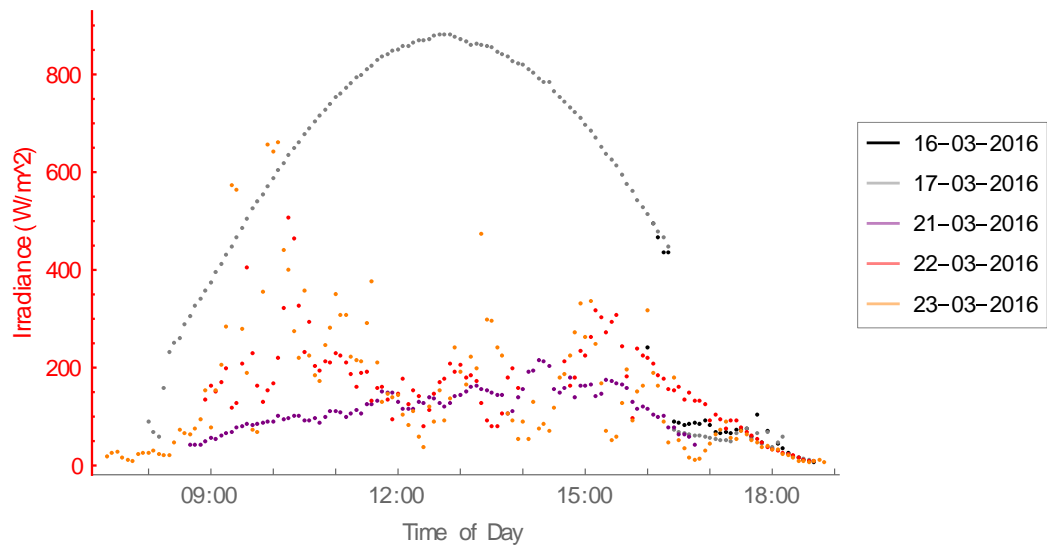


Figure 23: Irradiance over time on five measurement days

Indirect sunlight from the sky could cause the high APE with low irradiance trend; clouds or buildings obstruct direct light from reaching the panel, thus reducing the irradiance, and relatively bluer, ambient light is left to cause electron excitations in the panels. Figure 25 confirms this as it clearly displays the difference between irradiance and APE values of sunny days versus those of cloudy days.

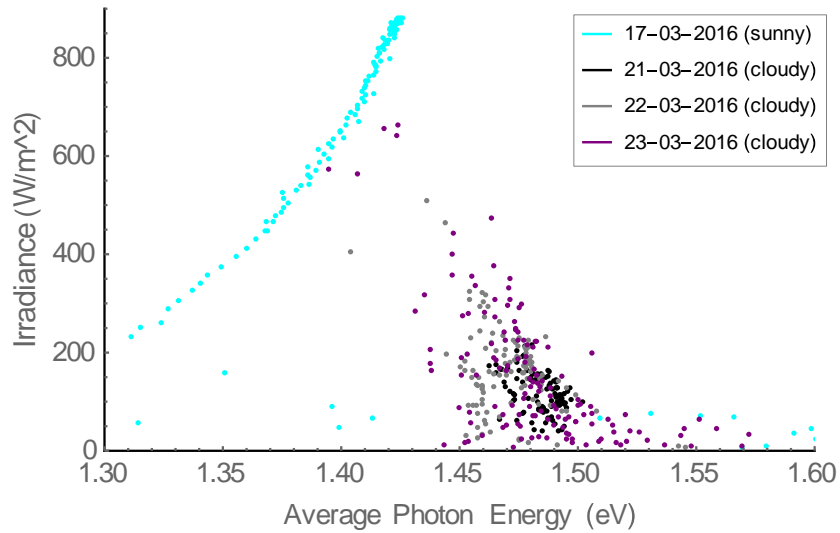


Figure 24: Average photon energy versus irradiance for one sunny and three cloudy days

Overall, the irradiance varies between 0 and 900 over whole days, showing the large differences in power throughout the day (Figures 25 and 26), with the irradiance always staying below the irradiance level of the standard test conditions which reaches 1000 W/m² as explained in Section 2.6 and peaks at 1500 W/m²/μm (Figure 18). This suggests that the current results will display variations with respect to the STC when calculating operating efficiencies of solar panels.

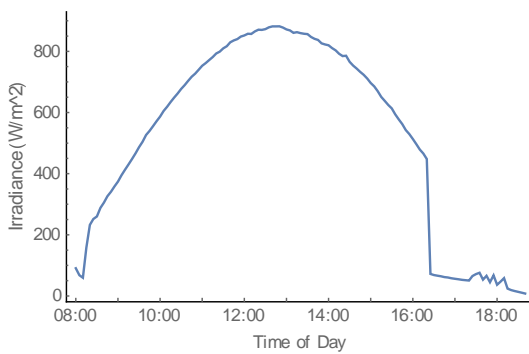


Figure 25: Irradiance over time on 17-03-2016

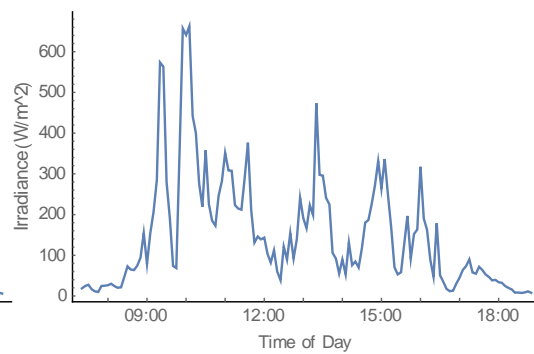


Figure 26: Irradiance over time on 23-03-2016

Figures 25 and 26 also show that the irradiance reacts rapidly depending on the weather conditions. On sunny days, such as 17-03-2016, the irradiance gradually increases and decreases with changing solar position, but on cloudy or rainy days, such as 23-03-2016, the incoming radiation is frequently obstructed by clouds and cannot reach the solar panels. Figure 27 depicts

a combination of these conditions or, in other words, of slightly cloudy days. Here it is clear that despite the increase in irradiance with solar position, large variations can occur due to other effects, mainly clouds.

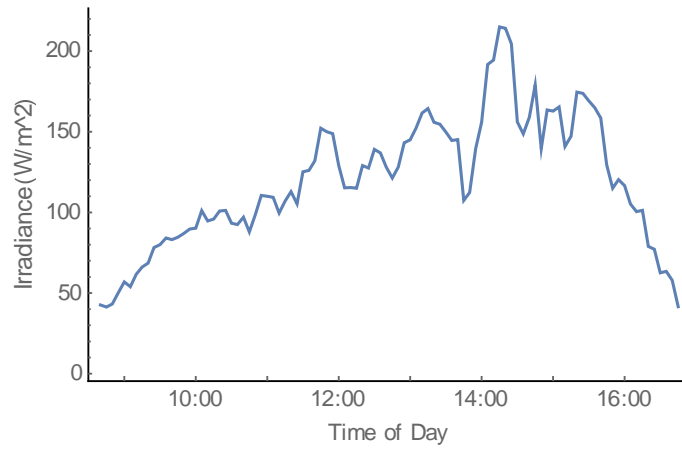


Figure 27: Irradiance over time on 21-03-2016

5.5. Weather Variations

The cloud cover varied widely during the days of measurement. This influenced the solar cell performance through spectrum and irradiance. However, multiple other weather factors were also investigated with the weather station – temperature and relative humidity mainly. Figures 28 to 32 show the variation in the weather data collected over the six days of measurement.

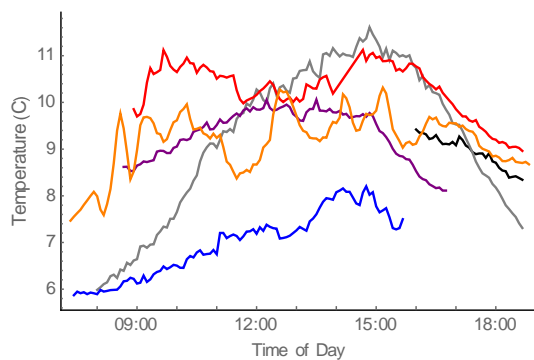


Figure 28: Temperature over time

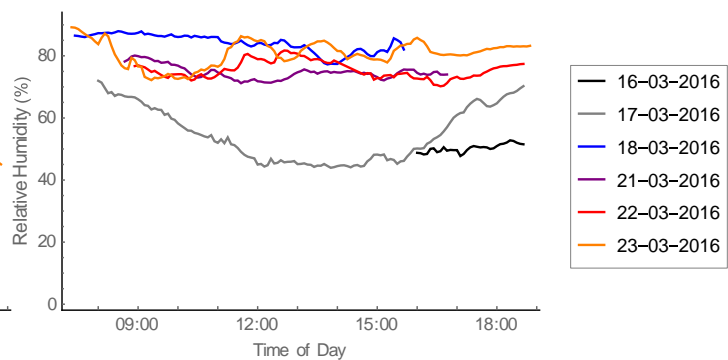


Figure 29: Relative humidity over time

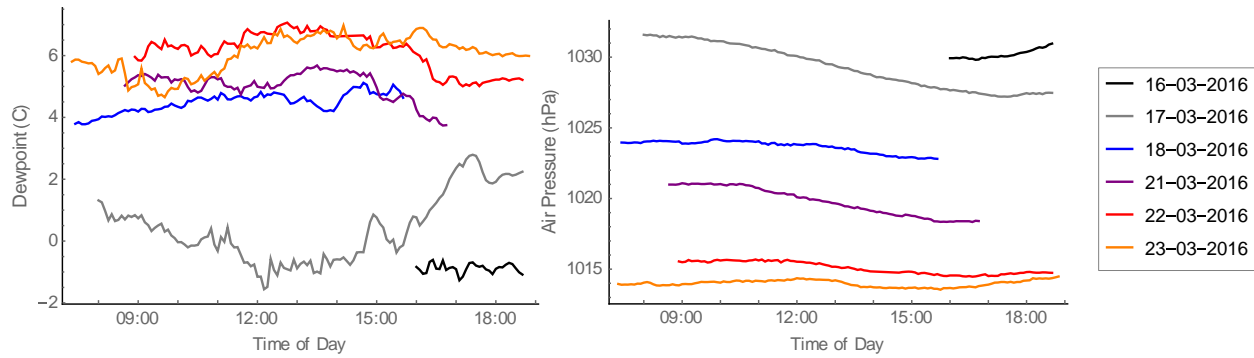


Figure 29: Air pressure over time

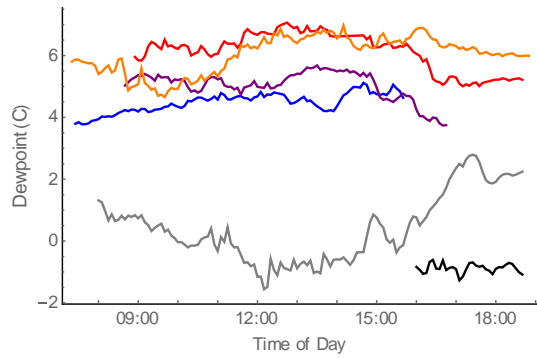


Figure 30: Dew point over time

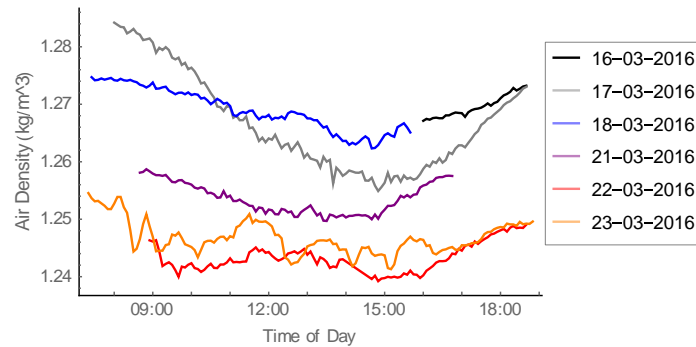


Figure 30: Air density over time

The temperature follows the expected pattern with a peak in the afternoon and steady decline before and afterwards. The variability of the temperature can, however, still be relatively large which is most likely due to a reduction in sunlight reaching the solar panels as clouds pass by. The humidity tends to be relatively constant with the exception of 17-03-2016, which was a sunny day (see Section 5.4); this is also the day with the largest temperature variation. This trend of relative humidity can also be seen in Figure 29 wherein 17-03-2016 also has the largest difference during the day.

5.6. Best Performing Solar Panel

The various bandgaps of solar panels result in different responses to the incoming spectra (see Section 5.3) and small bandgap panels are thus more likely to perform better at low energy spectra than large bandgap solar cells. The module temperature (see Section 5.2) also influences the performance and these two factors, the spectra and the module temperature, enable for the calculation of the Shockley-Queisser limits at any point in time of measurement (Figures 33 to 38). The CdTe panel has a significantly different response to some points in time compared to the other five panels. This will be further investigated in Section 5.7.

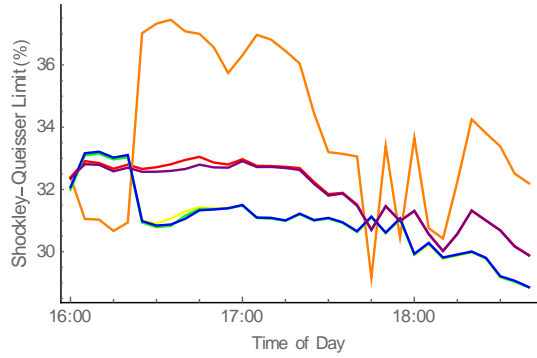


Figure 31: SQ limit over time on 16-03-2016 (late afternoon)

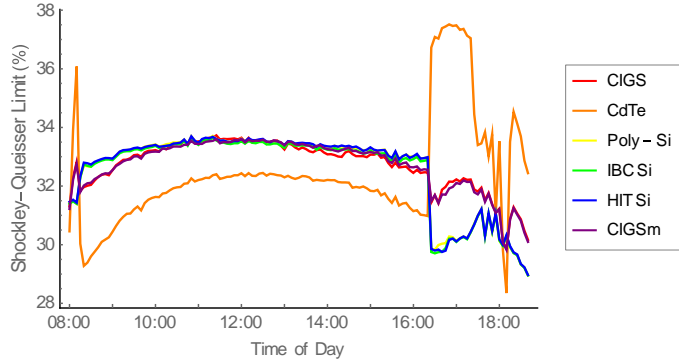


Figure 34: SQ limit over time on 17-03-2016

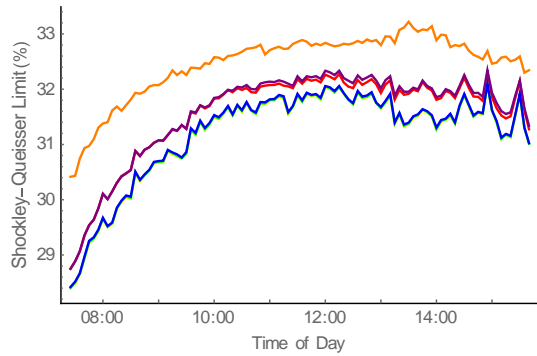


Figure 32: SQ limit over time on 18-03-2016

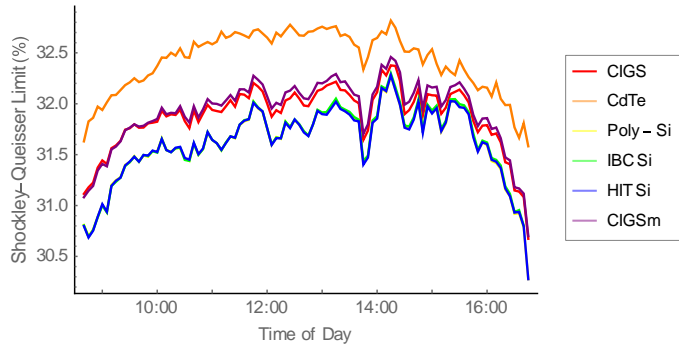


Figure 33: SQ limit over time on 21-03-2016

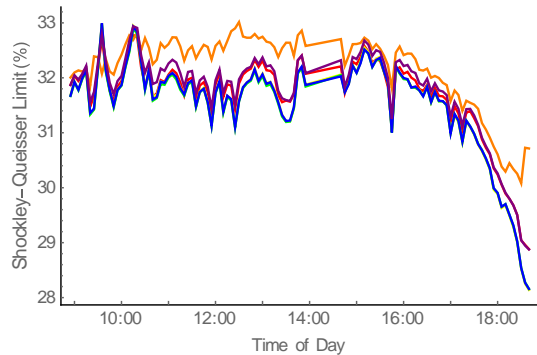


Figure 34: SQ limit over time on 22-03-2016

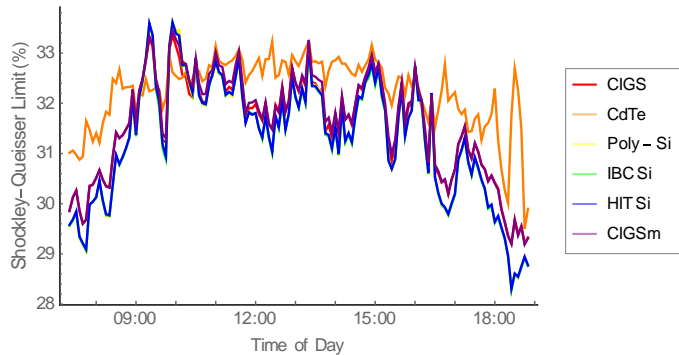


Figure 35: SQ limit over time on 23-03-2016

In these figures it is clear that module 2, CdTe, is generally expected to have a higher efficiency than the other modules. Furthermore, the calculated value of its SQ limit responds quite differently to spectrum changes as is especially clear in Figures 33 and 34, but also comes across in the small SQ differences with the other panels on the remaining days. The measured efficiency shows different trends, however (Figures 39 to 44). Despite the similar bandgaps modules 1 and 6, which are both CIGS panels, have significantly lower performances than modules 3 to 5, which are silicon based panels.

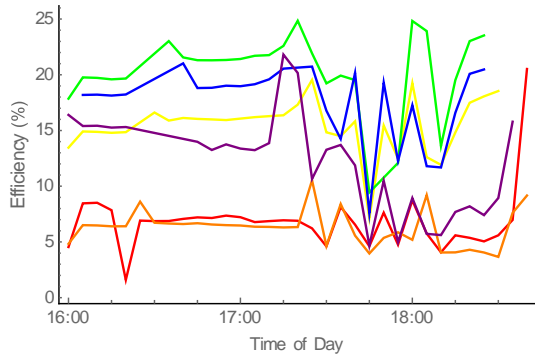


Figure 39: Observed efficiency over time on 16-03-2016

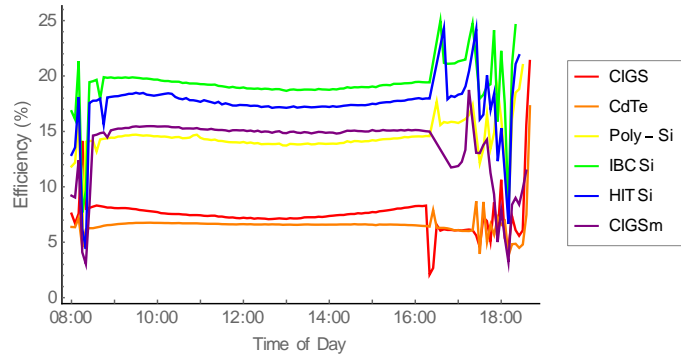


Figure 40: Observed efficiency over time on 17-03-2016

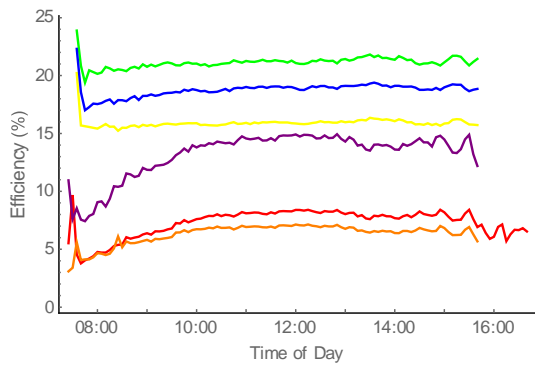


Figure 41: Observed efficiency over time on 18-03-2016

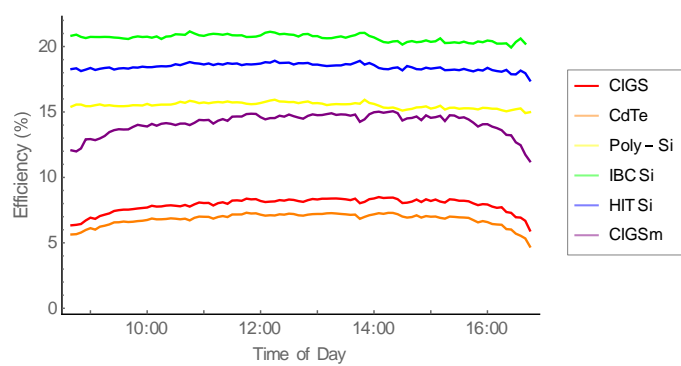


Figure 42: Observed efficiency over time on 21-03-2016

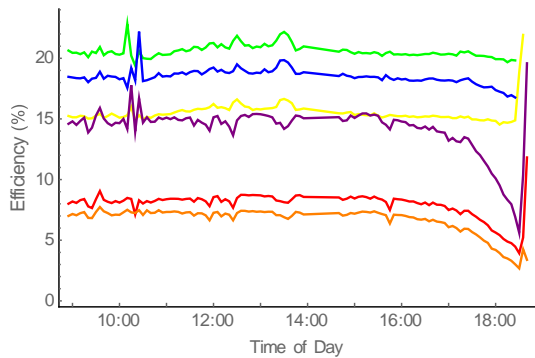


Figure 36: Observed efficiency over time on 22-03-2016

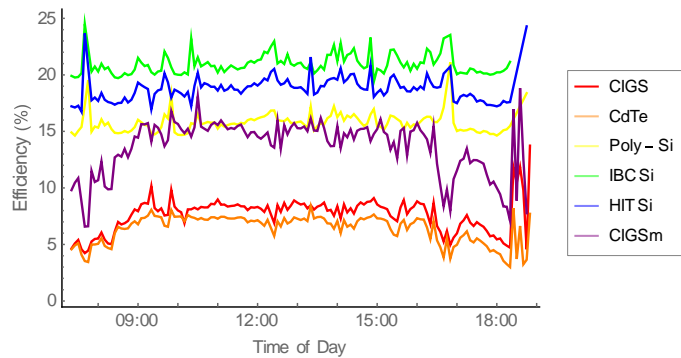


Figure 37: Observed efficiency over time on 23-03-2016

Most days show a general trend in both Shockley-Queisser limit and efficiency wherein the value starts off low, steadily increases, and later gradually declines again. This is thus most likely caused by the solar position which causes diffuse spectra with low intensity at large solar angles, low sun, and more direct and high intensity spectra at smaller angles. Figure 40 shows a different efficiency curve with a slight low in the middle of the day. However, the SQ limit of that day does not display the same pattern. Therefore, spectrum and module temperature cannot explain this phenomenon. A possibility is a difference in irradiance values as measured by the pyranometer and the spectrometer; however, this is unlikely as Figure 10 shows few

outliers. Outliers in the efficiency data can mainly be found at the beginning and end of the day. Section 6.1 will provide an explanation for this.

The IBC silicon panel, consistently has a higher observed efficiency, while the HIT module and the Poly-Si module average second and third on all days. The CIGSm module achieves efficiencies close to the Poly-Si one and on sunny days even surpasses the efficiencies of this module. Module 1, CIGS, and 2, CdTe, have the lowest efficiencies, between 5% and 10%. The relative performance of the solar panels – the difference in SQ and efficiency over the SQ limit – makes clear that the CdTe panel is not operating nearly as well as its potential would suggest (Figure 45).

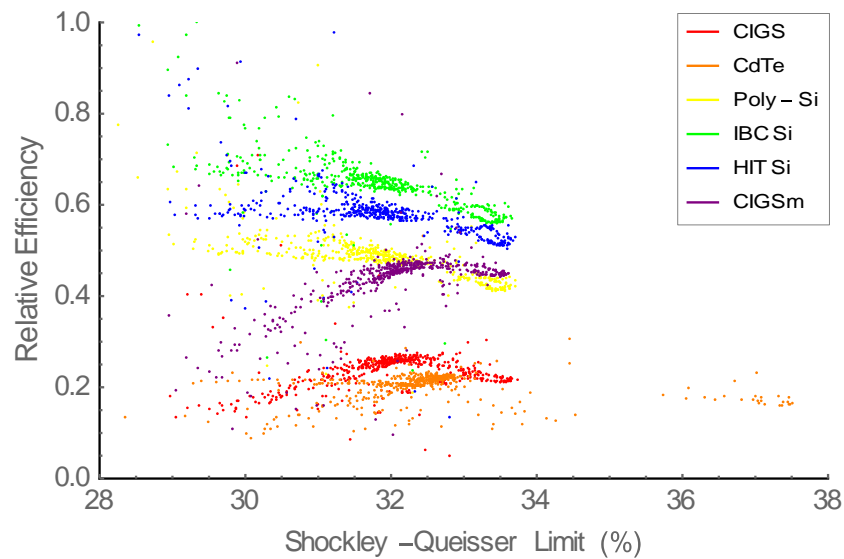


Figure 38: Shockley-Queisser limit versus relative efficiency

5.7. Influence of Average Photon Energy

Different behaviour can be observed in Figures 46 and 47, which show the correlation between the average photon energy (APE) and the efficiency and SQ limit, respectively. There is a sharp increase in the SQ limit as the APE approaches 1.42 eV followed by a sharp decline until 1.5 eV. Hereafter, the SQ for CdTe gradually grows with increasing average photon energy while the other – small bandgap – solar panels have an almost flat relation between APE and SQ with a peak around 1.75 eV. This is due to the larger bandgap of CdTe, 1.45 eV; the smaller bandgap materials will waste the excess amount of energy in the photons, while the CdTe will not do so to the same extent.

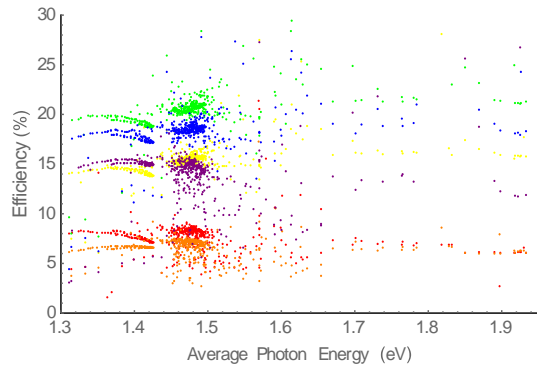


Figure 39: Average photon energy versus observed efficiency

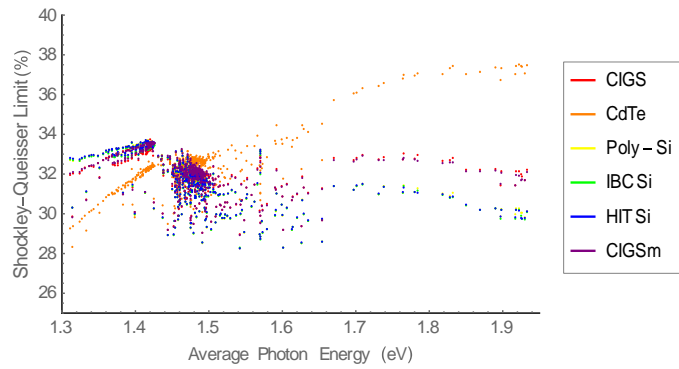


Figure 40: Average photon energy versus SQ limit

The observed efficiency has a different relation with the APE: for all panels the efficiency starts off flat and then decreases, followed by a jump in efficiency with increasing APE after the 1.42 eV mark. After 1.5 eV the correlation becomes unclear through trendless data points. However, the limited data in this region appears to show no further changes in the efficiency.

5.8. Influence of Relative Humidity

Even though H₂O molecules, as explained in Section 3.1, scatter light at certain wavelengths and thus influence the spectra, the following figures show that there is no significant impact of the relative humidity on the measured efficiency (Figures 48 and 49). A possible explanation is given in Section 6.1.

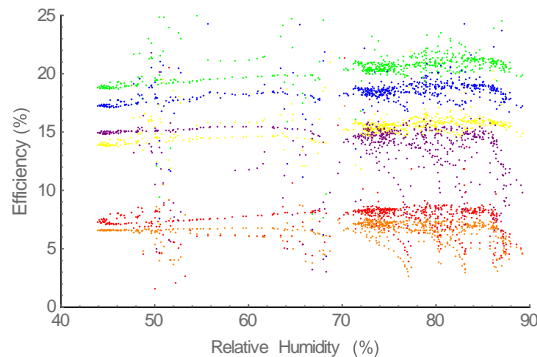


Figure 41: Relative humidity versus observed efficiency

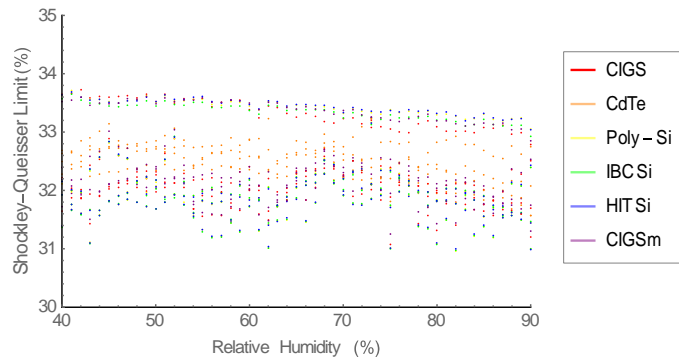


Figure 49: Relative humidity versus SQ limit

6. Discussion and Conclusion

6.1. Environmental Conditions

From the figures on temperature (Figures 11 and 12) it becomes clear that there is no clear dependence on temperature in measured efficiency and even a minor increase in the case of the SQ limit despite the fact that theory predicts a negative correlation (Section 2.3). This suggests that at low operating temperatures, below 35 °C, an increased module temperature might actually be favourable for solar cell performance (potentially because it coincides with a solar spectrum that is more favourable). However, Figures 13 and 14 also show that higher irradiance values are associated with higher efficiencies, especially from very low light intensity (around 0 W/m²) towards low light intensity (200 W/m²). In Figure 13 this is mostly visible in the case of the CIGS panels and in figure 14 the SQ limits all show a sharp increase at low irradiance values. A larger irradiance also increases the temperature and the irradiance might thus also contribute to the unexpected temperature effect. On sunny days, this is also partly due to higher APE values at larger light intensity which increase the SQ limit of all six solar panels (Figure 47). However, on cloudy days the irradiance is low and the associated APE is high (Figure 25), which results in clear differences in SQ limit between the different materials.

6.2. Observed Efficiency versus Shockley-Queisser Limit

CdTe displays larger SQ values than the CIGS- and silicon-based panels. This is due to the larger bandgap (1.45 eV) of the former material compared to the smaller bandgaps (1.12 and 1.2 eV, respectively) of the latter two materials. The same trend is not visible for the observed efficiency (Figure 46), which indicates that more factors than just the module temperature, bandgap, and APE influence efficiency. The different relation between the observed efficiency and APE compared to the SQ case might come about through two mechanisms: reflection and calculation. An increased reflection at certain wavelengths, that is not accounted for here, would change the energy of absorbed photons, which in turn would change the efficiency. The difference between calculated irradiance, by integrating over the incoming spectrum, in the case of SQ limits, and measured irradiance from the pyranometer in the case of observed efficiencies, might also explain the mismatch between these two types of efficiency. However, this was disproven in Section 5.1.

6.3. Dutch humidity

The relative humidity of the Dutch climate shows no clear impact on the performance – in both SQ limit and observed efficiency – of the solar panels. This is most likely due to the fact that relative humidity in this study was measured at ground level while the scattering of light due to water vapour takes place higher in the troposphere in the presence of clouds (Hobbs 2000).

Therefore, it is suggested that the level of humidity at ground level in a climate shows no measurable effect on the performance of solar cells.

6.4. Outliers

Outliers in the efficiency data (Figures 39 to 44) might be caused by a slight difference in time of measurement between the pyranometer and spectrometer and the six solar panels. In this way a passing cloud could affect the panels and measurement equipment at different times, causing a discrepancy. The latter causes partial shading of the solar field and might thus prevent the light from reaching the pyranometer while still allowing for the solar panels to generate power.

6.5. Comparing Solar Panels

As previously mentioned in Section 5.6, the IBC Si panel consistently shows the largest observed efficiency values with the other silicon panels having the second and third largest efficiencies in general (HIT Si and Poly-Si, respectively). There is also a difference between the two CIGS panels despite them being made of the same material; the latter performs better by at least a few percent. This can be attributed to the reflective back surface of the module that allows for more light absorption in the thin film material and possible to the reduced quality of the substrate in the case of a flexible panel, such as the CIGS panel. The reflective back surface was also accounted for by the manufacturers in stating the panels' efficiencies (Table 1). The CdTe panel performs much worse than its SQ limit would suggest (Figure 45). This is due to the fact that the four CdTe panels, of which one is measured, are broken due to mechanical stress and strain when attached to the metal solar field frame. Another possible explanation of the poor efficiency could have been the low Voc from CdTe panels (Polman et al. 2016), which was already accounted for in the efficiency value as stated by the manufacturer (Table 1). Overall, IBC Si is performing at highest efficiencies, which is also in line with the efficiencies as stated by the manufactures (Table 1), and can thus be considered the best panel when only considering amount of power generation. However, the IBC Si panel might be quite expensive and other panels might prove to be more cost-beneficial. CdTe shows potential at high APE values (Figure 47), but due to the low irradiance values associated with these average photon energies it might not be cost-beneficial to invest in optimising CdTe for these circumstances.

6.6. Limitations

As the setup of the AMOLF solar field only completely started during January 2016, many technical difficulties arose during the measurement period. These resulted in a significantly smaller amount of data than initially intended. Among these technical issues were the electrical wiring and a few broken panels. The latter resulted in the reported CdTe data to originate in a broken panel as all four available were damaged before measurement could start. This affected the performance of this solar panel type and should thus be considered in evaluating the different panels. As CdTe has a near ideal bandgap and there was only one type of this material,

this was a significant limitation to this study. The wiring of the solar field had to be reapplied halfway through February due to extremely high voltages, resulting in sparks and thus danger for the operators of the field. This caused irregular measurement to take place in addition to a short measurement period. In future projects with the solar field this can now be prevented. As previously mentioned (Section 3.1), precipitation is a large component of the Dutch weather. The weather station at AMOLF did, however, not allow for direct measurement of this weather condition. Humidity and low irradiance substituted for rain instead, but high humidity and low irradiance do not necessarily correspond to precipitation. This could be avoided with a different weather station. Another aspect of the Dutch climate that is not fully incorporated in this report is due to the short time span of the experiment; only late-winter and early-spring data is included. To be able to conclude on the influence of the Dutch climate on solar cell performance, research should be conducted for the entire year. A last limitation, which was touched upon in previous sections, is the absence of reflection measurement. The amount of reflection from the solar panels might vary between different wavelengths; this in turn influences the solar cell performance. In this report, reflection was not accounted for while it could explain the dissimilar observations in SQ limit and observed efficiency (Figures 46 and 47).

6.7. Conclusion and Future Research

The climate of the Netherlands is vastly different from climates mainly investigated for solar energy due to its high levels of relative humidity and low values of irradiance. However, most panels examined in this report still show reliable efficiencies. The Dutch weather, furthermore, displays an interesting trend: low irradiance values are correlated with high average photon energies. These data points are associated with cloudy circumstances where the blue light of the sky was the main driver of photogenerated current. At these moments, CdTe panels show the increasing SQ limits due to the high bandgap of the semiconductor material, while the CIGS and silicon panels follow a declining trend due to their smaller bandgaps. The Dutch climate would thus, due to its large amount of cloudy days, be more suited to CdTe if these were optimised for this type of weather. However, due to the low irradiance values associated with this weather type, it might not be cost-beneficial to pursue this development. The IBC Si panel consistently performs at highest efficiencies – as predicted by the solar panel manufacturers – and could thus still be considered the best option (when considering power generation and ignoring possible high prices) for climates such as the one in the Netherlands despite its lower SQ limit values in cloudy weather. The influence of Dutch weather and climate over larger timescales should, however, be examined in order to be certain of these conclusions. The solar field at FOM Institute AMOLF could be the basis for this research wherein the technical difficulties of this first project could be avoided, creating more reliable results on longer timescales. Next steps could also explore the performance of solar panels in more climate systems, such as cold climates or continental climates, to find the types of solar cells with the highest efficiencies. This could lead to a more cost-beneficial contribution of solar energy to the global energy market and in turn to a more sustainable future.

6.8. Acknowledgements

This study would not have been possible without the help of Bruno Ehrler, co-supervisor of this project and group leader at FOM Institute AMOLF. He offered help in both understanding theoretical background and completing the project smoothly. Thanks also to Moritz Futscher for making the time to help solving spectrum and Shockley-Queisser calculations. Furthermore, my gratitude towards the support staff of AMOLF – especially Ivo Klinkert, Mathijs van Lindenberg, and Dion Ursem –, who offered their enthusiasm and expertise and enabled the project to conclude in time. Lastly, I want to acknowledge the great support of Forrest Bradbury, as a supervisor, teacher, and tutor.

Bibliography

- Ashcroft NW, Mermin ND. 1976. Solid state physics. New York: Holt, Rinehart and Winston.
- Averill B, Eldredge P. 2011. Principles of General Chemistry. Creative Commons. Retrieved from: <http://2012books.lardbucket.org/books/principles-of-general-chemistry-v1.0/index.html>.
- Compendium. 2015. Meteorologisch gegevens, 1990 – 2014 [Internet]. [cited 2016 Apr 15]. Available from: www.compendiumvoordeleefomgeving.nl
- Emziane M, Altal F. 2012. Orientation, air-mass and temperature effects on the optimal power output of stationary photovoltaic modules in the GCC region. *International Journal of Ambient Energy*. 33:209–213. DOI: 10.1080/01430750.2012.711082
- Ehrler B. 2012. Nanocrystalline Solar Cells. PhD Thesis, University of Cambridge, Cambridge (UK)
- Hanna MC, Nozik AJ. 2006. Solar conversion efficiency of photovoltaic and photoelectrolysis cells with carrier multiplication absorbers. *J Appl Phys Journal of Applied Physics*. 100. DOI: 10.1063/1.2356795
- Hobbs PV. 2000. Introduction to atmospheric chemistry: a companion text to Basic physical chemistry for the atmospheric sciences. Cambridge: Cambridge University Press.
- Kaldellis JK, Kapsali M, Kavadias KA. 2014. Temperature and wind speed impact on the efficiency of PV installations. Experience obtained from outdoor measurements in Greece. *Renewable Energy*. 66:612–624. DOI: 10.1016/j.renene.2013.12.041
- KNMI (Royal Dutch Meteorological Institute). 2011. Klimaatatlas. Noordhoff Atlasproducties [Internet]. [cited 2016 Apr 15]. Available from: www.klimaatatlas.nl
- Kottek M, Grieser J, Beck C, Rudolf B, Rubel F. 2006. World Map of the Köppen-Geiger climate classification updated. *Meteorologische Zeitschrift Meteorol Z*. 15:259–263. DOI: 10.1127/0941-2948/2006/0130
- Shaltout MM, El-Nicklawy M, Hassan A, Rahoma U, Sabry M. 2000. The temperature dependence of the spectral and efficiency behavior of Si solar cell under low concentrated solar radiation. *Renewable Energy*. 21:445–458. DOI: 10.1016/S0960-1481(00)00075-6
- Neamen DA. 2012. Semiconductor physics and devices: basic principles. Boston: McGraw-Hill.

National Renewable Energy Laboratory (NREL). Device Performance Measurement. NREL: Measurements and Characterization - [Internet]. [cited 2016 Apr 15]. Available from: http://www.nrel.gov/pv/measurements/device_performance.html

Peel MC, Finlayson BL, McMahon TA. 2007. Updated world map of the Köppen-Geiger climate classification. *Hydrology and Earth System Sciences Discussions Hydrol Earth Syst Sci Discuss.* 4:439–473. DOI: 10.5194/hessd-4-439-2007

Perez R, Perez M. 2009. A fundamental look at the energy reserves for the planet. IEA/SHC Solar Update. Retrieved from: Research Gate.

Piliougine M, Carretero J, Mora-López L, Sidrach-De-Cardona M. 2011. Experimental system for current-voltage curve measurement of photovoltaic modules under outdoor conditions. *Prog Photovolt: Res Appl Progress in Photovoltaics: Research and Applications.* 19:591–602. DOI: 10.1002/pip.1073

Polman A, Knight M, Garnett EC, Ehrler B, Sinke WC. 2016. Photovoltaic materials: Present efficiencies and future challenges. *Science.* 352(6283). DOI: 10.1126/science.aad4424

Honsberg C, Bowden S (PV Education). 2013. PVEducation [Internet]. [cited 2016 Apr 15]. Available from: <http://pveducation.org/>

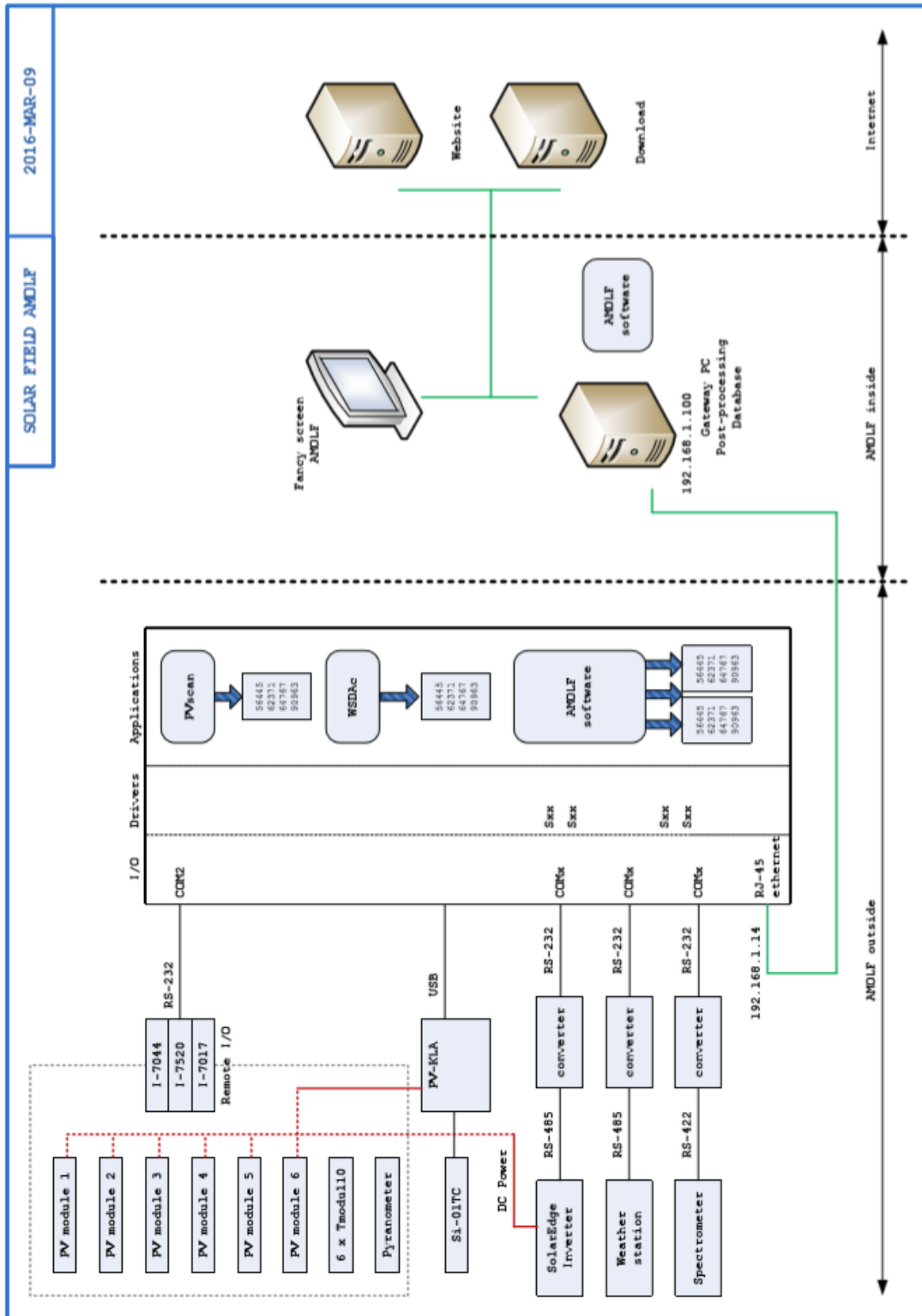
Sargent EH. 2012. Colloidal quantum dot solar cells. *Nature Photonics Nature Photon.* 6:133–135. DOI: 10.1038/nphoton.2012.33

Saetre TO, Midtgård O-M, Yordanov GH. 2011. A new analytical solar cell I–V curve model. *Renewable Energy.* 36:2171–2176. DOI: 10.1016/j.renene.2011.01.012

Shockley W, Queisser HJ. 1961. Detailed Balance Limit of Efficiency of p-n Junction Solar Cells. *J Appl Phys Journal of Applied Physics.* 32. DOI: 10.1063/1.1736034

Touati FA, Al-Hitmi MA, Bouchech HJ. 2013. Study of the Effects of Dust, Relative Humidity, and Temperature on Solar PV Performance in Doha: Comparison Between Monocrystalline and Amorphous PVS. *International Journal of Green Energy.* 10:680–689. DOI: 10.1080/15435075.2012.692134

Appendix 1: Data Collection Circuit and Software System Overview



Appendix 2: Mathematica Code

Dutch Solar Cell Performance

The efficiency and Shockley-Queisser limits of various solar panels under Dutch weather conditions

Ruby de Hart, 2016

Based on work by Bruno Ehrler and Moritz Futscher

Efficiency Calculations and Environmental Correlations - Ultimate Parameter List

■ Functions

Constants

Area definition

Definition Formulae

Weather Definition

Experimental Efficiency Calculation

```
*)*)*) ObsEFF [Pmpp, Area_, Opvnanometex_] := Pmpp / Area / Opvnanometex * 100
(*ObservedEfficiency = Pmpp / Opvnanometex * 100*)
ObsEFFtime [parametertime_, ExpezEFF_] := Table[{parametertime[[1, 1]], ExpezEFF[[1, 1]]}, {1, 1, Length[parametertime]}] (*observed efficiency against times)
```

Calculate Flux

Planck Current

Average Photon Energy Function

```
*)*)*) APE [input_, start_, end_] := Quiet[
spectral = Interpolation[input];
spectra2 = Interpolation[Table[{s, spectral[s] * s}, {s, input[[1, 1]], input[[-1, 1]]}]];
NIntegrate[spectral[w1], {w1, start, end}] / NIntegrate[spectra2[w1], {w1, start, end}] * fac
*)*)*)
```

Shockley - Queisser Limit Calculation

Spectra

SQ

```
*)*)*) SQ [Eg1_, Temp_, spectrum_, irradiance_, number_] := Quiet[
F[Eg1] := Interpolation[makeFlux[spectrum]][Eg1];
powerofsun := irradiance[[number]] * 1000;
J0[Eg1] := NIntegrate[F[Eg1], {Eg, Eg, 4.1}];
JR[Eg1, V_] := q * 2 * Pi / (c^2 * h^2 * 3) * NIntegrate[Eg^2 / (Exp[(Eg - V) / (k * Temp)] - 1), {Eg, Eg, 4.1}];
jg = J0[Eg1];
d = Table[{v1, jg - JR[Eg1, v1]}, {v1, 0, Eg1, .005}];
iv = Interpolation[d];
voo = FindRoot[iv[v], {v, .5}][[1, 2]];
jso = J0[Eg1] - JR[Eg1, 0];
(* Finding the maximum conversion efficiency *)
NMaximize[{100 iv[v] / powerofsun, d[[1, 1]] < v < d[[-3, 1]]}, v][[1, 1]]
*)*)*)
```

Separation Formulae

■ Weather

■ Observed Efficiency

■ Spectra

Spectra 16-03-2016

Spectra 17-03-2016

Import and Incorporating IR

```
IN791= SetOptions[Interpolation, InterpolationOrder -> 1]
      (InterpolationOrder -> 1, Method -> Automatic, PeriodicInterpolation -> False)
OUT91= {InterpolationOrder -> 1, Method -> Automatic, PeriodicInterpolation -> False}
OUT92= {InterpolationOrder -> 1, Method -> Automatic, PeriodicInterpolation -> False}
```

Spectrum Fit Function

```
IN792= SpectraFitPlanck1703[Input_, spectrumnumber_] := Quiet[
  spectra = Input[{"All", spectrumnumber}];
  spectrain = Interpolation[spectra];
  powerspectrum = Integrate[spectrain[w], {w, spectra[[1, 1]], spectra[[-1, 1]]}];
  spectracut = Table[{s, spectrain[s]}, {s, 350, 1050}];
  spectracutint = Interpolation[spectracut];
  FitPlanck = Fit[Table[{s, spectracutint[s]}, {s, 1000, 1050}], {IPlanck[5777, w]}, w];
  Addhigh = Join[
    Table[{s, FitPlanck /. w -> s}, {s, 1051, 1100}],
    Table[{s, Fit[{1100, FitPlanck /. w -> 1100}, {1130, FitPlanck / 100 /. w -> 1100}], {s, w} /. w -> s}, {s, 1101, 1130}],
    Table[{s, FitPlanck / 100 /. w -> 1100}, {s, 1131, 1131}],
    Table[{s, Fit[{1131, FitPlanck / 100 /. w -> 1100}, {1180, FitPlanck /. w -> 1180}], {s, w} /. w -> s}, {s, 1132, 1180}],
    Table[{s, FitPlanck /. w -> s}, {s, 1181, 1210}],
    Table[{s, Fit[{1210, FitPlanck /. w -> 1210}, {1350, 0}], {s, w} /. w -> s}, {s, 1211, 1350}],
    Table[{s, 0}, {s, 1351, 1420}],
    Table[{s, Fit[{1420, 0}, {1510, FitPlanck /. w -> 1510}], {s, w} /. w -> s}, {s, 1421, 1510}],
    Table[{s, FitPlanck /. w -> s}, {s, 1511, 1770}],
    Table[{s, Fit[{1770, FitPlanck /. w -> 1770}, {1810, 0}], {s, w} /. w -> s}, {s, 1771, 1810}],
    Table[{s, 0}, {s, 1811, 1950}],
    Table[{s, Fit[{1950, 0}, {2000, FitPlanck /. w -> 2000}], {s, w} /. w -> s}, {s, 1951, 2000}],
    Table[{s, FitPlanck /. w -> s}, {s, 2001, 2400}],
    Table[{s, Fit[{2400, FitPlanck /. w -> 2400}, {2500, 0}], {s, w} /. w -> s}, {s, 2401, 2500}],
    Table[{s, 0}, {s, 2501, 2900}],
    Table[{s, Fit[{2900, 0}, {3400, FitPlanck /. w -> 3400}], {s, w} /. w -> s}, {s, 2901, 3400}],
    Table[{s, FitPlanck /. w -> s}, {s, 3401, 4000}];
  ];
  Addlow = Table[{s, Fit[{300, 0}, spectracutint[s]], {s, w} /. w -> s}, {s, 300, 349}];
  spectrafit = Join[Addlow, Table[{s, spectracutint[s]}, {s, 350, 1050}], Addhigh];
  spectrafitint = Interpolation[spectrafit];
  powerspectrumfit = Integrate[spectrafitint[w], {w, spectrafit[[1, 1]], spectrafit[[-1, 1]]}];
];
```

Spectrum Fit and Plot

```
IN794= ultimatefits [spectrumnumber_] :=
  Quiet[SpectraFitPlanck1703[allspectra1703, spectrumnumber];
  FitPlanck = Fit[Join[Table[{s, spectracutint[s]}, {s, 1000, 1050}], {IPlanck[5777, w]}, w];
  unitsspectra = Table[{spectrafit[s, 1]}, spectrafit[[s, 2]] / 1000}, {s, 1, Length[spectrafit]}];
  surpower = Quiet[Integrate[Interpolation[unitsspectra][w], {w, unitsspectra[[1, 1]}, unitsspectra[[-1, 1]]}];
IN795= surpower1703 = Flatten[Table[ultimatefits[s], {s, 1, Length[allspectra1703[[1]]}]]];
IN796= ListLinePlot[{spectra, spectrafit}, PlotRange -> All]
```

Spectra Plots

APE

Spectra 18-03-2016

Spectra 21-03-2016

Spectra 22-03-2016

Spectra 23-03-2016

■ SQ Limit

■ Full Parameter List

```

10348) parameterlists[timeList, parList, obsEffList, SQList] := Flatten[Table[{Append[Append[Flatten[Append[{timeList[[i]], parList[[i]], 1}, obsEffList[[i]], SQList[[i]]], {1, Length[parList[[i]]}], 1];
10349) names = {"dateandtime", "modules", "spectrum", "weather"};
10350) parameterheaders = {"Vmpp", "Imp", "Pmp", "Voc", "FF", "GSI", "ModuleT", "Opvt", "Eff", "SQ"};
10351) weatherheaders = {"Temp", "Dewpoint", "Humidity", "Airpressure", "Airdensity", "Averagewindspeed", "Actualwindspeed", "Winddirection", "Windmeasurementquality"};
10352) headers = {names, parameterheaders, weatherheaders};

```

Input lists

Ultimate List making (with spectra)

```

103114) listmaking1603[rowNumber_] := {time1603[[rowNumber]], modules1603[[rowNumber]], spectrumlist1603[[rowNumber]], weatherlist1603[[rowNumber]]};
103115) listmaking1603[;;] // MatrixForm; (*stake all sublists of parList and weatherlist > creates a matrix with all parList elements on the first row and all weatherlist elements on the second row >
transpose is needed*)
ultimatelist1603 = Prepend[listmaking1603[;;], headers];
103117) listmaking1703[rowNumber_] := {time1703[[rowNumber]], modules1703[[rowNumber]], spectrumlist1703[[rowNumber]], weatherlist1703[[rowNumber]]};
103118) listmaking1703[;;] // MatrixForm;
ultimatelist1703 = Prepend[listmaking1703[;;], headers];
103120) listmaking1803[rowNumber_] := {time1803[[rowNumber]], modules1803[[rowNumber]], spectrumlist1803[[rowNumber]], weatherlist1803[[rowNumber]]};
103121) listmaking1803[;;] // MatrixForm;
ultimatelist1803 = Prepend[listmaking1803[;;], headers];
103122) listmaking2103[rowNumber_] := {time2103[[rowNumber]], modules2103[[rowNumber]], spectrumlist2103[[rowNumber]], weatherlist2103[[rowNumber]]};
103123) listmaking2103[;;] // MatrixForm;
ultimatelist2103 = Prepend[listmaking2103[;;], headers];
103124) listmaking2203[rowNumber_] := {time2203[[rowNumber]], modules2203[[rowNumber]], spectrumlist2203[[rowNumber]], weatherlist2203[[rowNumber]]};
103125) listmaking2203[;;] // MatrixForm;
ultimatelist2203 = Prepend[listmaking2203[;;], headers];
103126) listmaking2303[rowNumber_] := {time2303[[rowNumber]], modules2303[[rowNumber]], spectrumlist2303[[rowNumber]], weatherlist2303[[rowNumber]]};
103127) listmaking2303[;;] // MatrixForm;
ultimatelist2303 = Prepend[listmaking2303[;;], headers];

```

Obtaining data in Ultimate List - How to

Module parameters

Weather data

Parameter list - Time, APE, Modules, VWeather (without spectra)

16-03-2016

17-03-2016

```

103161) ultimateparametertable1703 = Table[{Vmpp1703[[i]], imp1703[[i]], pow1703[[i]], voc1703[[i]], isc1703[[i]], eff1703[[i]], tmodule1703[[i]], irradiancel1703[[i]], effe1703[[i]], SQ1703[[i]],
{1, Length[Vmpp1703[[i]]];
ultimateparametertable21703 = Table[{Vmpp21703[[i]], imp21703[[i]], pow21703[[i]], voc21703[[i]], isc21703[[i]], eff21703[[i]], tmodule21703[[i]], irradiancel21703[[i]], effe21703[[i]], SQ21703[[i]],
{1, Length[Vmpp21703[[i]]];
ultimateparametertable31703 = Table[{Vmpp31703[[i]], imp31703[[i]], pow31703[[i]], voc31703[[i]], isc31703[[i]], eff31703[[i]], tmodule31703[[i]], irradiancel31703[[i]], effe31703[[i]], SQ31703[[i]],
{1, Length[Vmpp31703[[i]]];
ultimateparametertable41703 = Table[{Vmpp41703[[i]], imp41703[[i]], pow41703[[i]], voc41703[[i]], isc41703[[i]], eff41703[[i]], tmodule41703[[i]], irradiancel41703[[i]], effe41703[[i]], SQ41703[[i]],
{1, Length[Vmpp41703[[i]]];
ultimateparametertable51703 = Table[{Vmpp51703[[i]], imp51703[[i]], pow51703[[i]], voc51703[[i]], isc51703[[i]], eff51703[[i]], tmodule51703[[i]], irradiancel51703[[i]], effe51703[[i]], SQ51703[[i]],
{1, Length[Vmpp51703[[i]]];
ultimateparametertable61703 = Table[{Vmpp61703[[i]], imp61703[[i]], pow61703[[i]], voc61703[[i]], isc61703[[i]], eff61703[[i]], tmodule61703[[i]], irradiancel61703[[i]], effe61703[[i]], SQ61703[[i]],
{1, Length[Vmpp61703[[i]]];
ultimateweathertable1703 = Table[{temperature1703[[i]], dewpoint1703[[i]], humidity1703[[i]], pressure1703[[i]], density1703[[i]], avgspeed1703[[i]], actspeed1703[[i]]}, {1, 4, Length[temperature1703]};
103162) ultimateparametertable1703 =
Table[{time1703[[i]], spelist1703[[i]], ultimateparametertable1703[[i]], ultimateparametertable21703[[i]], ultimateparametertable31703[[i]], ultimateparametertable41703[[i]],
ultimateparametertable51703[[i]], ultimateparametertable61703[[i]], ultimateweathertable1703[[i]]}, {1, 1, Length[ultimateweathertable1703]};
ultimateparametertable1703[[1]]; (* data at first time slot *)
ultimateparametertable1703[[1, 2]]; (* APE data at first time slot *)
ultimateparametertable1703[[1, 3]]; (* first time parameter data module 1 *)
ultimateparametertable1703[[1, 9]]; (* weather data first time slot *)
ultimateparametertable1703[[1, 9, 3]]; (* humidity first time slot *)

```

21-03-2016

22-03-2016

23-03-2016

Full Parameter List (without spectra)

Capstone Plots

- Module Temperature
- Irradiance, efficiency, and SQ
- Efficiency versus SQ
- Efficiency, SQ, and APE
- APE, Irradiance, and Power
- Humidity
- Weather

Appendix 3: Data List Layout

